Supporting Information

Engineering electronic structure of Ni-Co bimetallic sites toward excellent electrochemical biomass upgrading and CO_2 reduction

Qing-Lian Yan [a], Xun-Bin Lin [a], Ji-dan Liu [a], Ting Ouyang [a]*, Zhao-Qing Liu [a, b]*

[a]*School of Chemistry and Chemical Engineering/Institute of Clean Energy and Materials/Key Laboratory for Clean Energy and Materials/Huangpu Hydrogen Innovation Center, Guangzhou University, Guangzhou 510006, P. R. China.*

[b]*School of Chemistry, South China Normal University, Guangzhou 510006, P. R. China.*

E-mail address: ouyt@gzhu.edu.cn; lzqgzu@gzhu.edu.cn (Z. Q. Liu)

1. Experimental Section

1. 1. Materials and analysis methods

All chemicals were commercially obtained and used without further purification and the detailed information of materials is shown in Supporting Information. The analysis methods are shown in Supporting Information.

1.2. Preparation of catalysts

1.2.1. Preparation of NiO, Co_3O_4, NiCoO and $NiCo_2O_4$/CC

The reactants of $Ni(NO_3)_2 \cdot 6H_2O$ (1 mmol), $Co(NO_3)_2 \cdot 6H_2O$ (2 mmol) and $CO(NH_2)_2$ (10 mmol) were dissolved in 50 mL of DI water and stirred thoroughly to form a homogeneous pink solution. After that, the solution was transferred to a stainless Teflon-lined autoclave of 100 mL inner volume, and a piece of the CC (1×3 cm^2) was vertically immersed into the mixture. Then the autoclave was sealed and placed in an electric oven set at a temperature of 120 °C for 8 h. After the reaction, the CC with deep pink precursor product evenly covering the surface was collected, which was washed repeatedly with DI water and ethanol to remove the residues. Finally, to achieve a chemical transformation to $NiCo_2O_4$, the precursor grown on carbon fiber cloth was then annealed at 350 °C in air atmosphere for 2 h. The different crystal structure electrodes were prepared by adjusting the ratio of nickel nitrate hexahydrate and cobaltous nitrate hexahydrate to 1:0, 0:1, and 1:1, to obtain the NiO, Co_3O_4, and NiCoO electrodes, respectively.

1.2.2. Preparation of Au/CC

Au nanoneedle arrays were grown on carbon cloth 1×3 cm^2. Au nanoneedle arrays were synthesized by three-electrode system with silver chloride (Ag/AgCl) as the reference electrode and Pt sheet as the counter electrode. The growth of Au nanoneedles was carried out in 0.5 M HCl and 160 mM $HAuCl_4$ at a constant potential (-0.4 V *vs*. RHE) for 300 s. The obtained Au nanoneedle array was taken out and thoroughly rinsed with ethanol and distilled water.

1.3. Characterizations

The morphology and microstructure of the as-prepared electrodes were investigated via field emission scanning electron microscopy (SEM, Phenom Nano G2, Holland) at an acceleration voltage of 15 kV and transmission electron microscopy (TEM, JEM-F200, JEOL, Japan). High-angle annular dark-field scanning transmission electron microscopy (HAADF-STEM) and energy-dispersive X-ray spectroscopy (EDS) mapping were taken on Thermo Fisher Scientific-Titan ETEM G2 operated at 200 kV, equipped with a probe aberration-corrector (AC) to improve the resolution of images. The crystal phase of the samples was characterized via X-ray diffraction (XRD, Bruker D8 Advance, Germany) using Cu Kα radiation at a scanning rate of 10° min^{-1} in the 2θ from 10° to 80° and the operating current and voltage were 40 kV and 40 mA, respectively. The X-ray photoelectron spectroscopy (XPS) measurements were carried out by Thermo escalab (250XI, America). The samples were irradiated with monochromatic Al-Kα radiation. Survey scans were performed using a step size of 0.1 eV per step. Binding energy was calibrated by the C 1s peak (284.8 eV) as a reference. The spectra were processed and analyzed by the

software code Athena.

1.4. In-situ Fourier transform infrared spectroscopy

The in-situ Fourier transform infrared spectroscopy (FT-IR) measurements were conducted at Nicolet iS50 (Thermo Scientific) instrument based on the absorption mode equipped with a Mercury Cadmium Telluride (MCT) detector in an atmosphere cooled by liquid nitrogen.

1.5. In-situ Raman spectroscopy

In-situ Raman spectra were collected using an in Via-Reflex laser Raman spectrometer (Renishaw, UK) equipped with a 50× long-working-distance objective lens. A 532 nm solid-state laser was used as the excitation source, operating at 20% of its maximum power intensity (approximately 25 mW at the sample surface). The spectra were acquired with an exposure time of 10 s per accumulation, and each measurement was repeated twice to improve the signal-to-noise ratio.

1.5. Electrochemical test

The electrochemical measurements were conducted using a standard threeelectrode system configuration on CHI760E electrochemical workstation (CH Instruments, Ins. Shanghai, China). Platinum electrode and Hg/HgO electrode were used as counter electrode and reference electrode, respectively. 1 M KOH or 1 M KOH + 1 M HMF was used as electrolyte. Linear sweep voltammetry (LSV) measurement was conducted at a scan rate of 5 mV s^{-1}. Presented potentials were normalized to reversible hydrogen electrode (RHE) according to the equation: $E_{RHE} = E_{Hg/HgO} + 0.059 \times pH + 0.098$. The LSV measurement results were fitted and calculated to obtain the Tafel slope. The equation formula of the Tafel curves is: $\eta = a + b \times \log |j|$. η represents the overpotential (RHE), b represents the Tafel slope and j is the current density. Cyclic voltammetry (CV) experiments were conducted in non-Faradic current region with different scanning rates from 2 to 10 mV s^{-1} to determine the double layer capacitances (C_{dl}) values of the catalysts. The electrochemical surface area (ECSA) normalized current density was calculated as:

ECSA-normalized current density = current density × C_s/C_{dl}

where C_s is the specific capacitance. 0.04 mF cm^{-2} was adopted as the value of C_s based on previous reports.

The stability measurements were carried out using chronopotentiometry measurement at a constant working potential.

In operando electrochemical impedance spectroscopy (EIS) tests spanned a frequency range of 10^{-2} to 10^5 Hz at various potentials in 1 M KOH and 1M KOH with PA, with an AC amplitude of 5 mV.

1.6. Calculation method

1.6.1. Products analysis:

High performance liquid chromatography instrument (HPLC, Agilent 1260 Infinity Series, USA) with an ultraviolet-visible (UV-Vis) detector and an Agilent Zorbax SB-C18 (150 mm × 4.6 mm, 5 μm) column was carried out to detect organic molecules containing 5-Hydroxymethylfurfural (HMF) and related oxidation products. The procedure was as follows: 25 μL of solution was taken out from the

electrolyte after reaction, diluted with 950 μL of deionized water, and then neutralized with 25 μL of 0.5 M H_2SO_4 solution. Subsequently, 10 μL of the above solution was removed for product analysis. The mobile phases A and B were ammonium formate and methanol, respectively.

The theoretical charge of HMF oxidation reaction was calculated by the following formula:

$6 \times (1.6\times10^{-19}\ C) \times 0.015\ L \times (0.0077\ mol\cdot L^{-1}) \times (6.02\times10^{23}\ mol\cdot L^{-1}) = 66.9\ C$

The conversion, yield and Faraday efficiency were calculated as follows:

HMF conversion (%) = [n (consumed HMF)/n (initial HMF)] ×100%

FDCA yield (%) = [n (generated FDCA)/n (initial HMF)] ×100%

Faraday efficiency (%) = [n (generated FDCA)/(Charge/(6×F))] ×100%

Where n was the molar amount of the reactant, calculated from HPLC data, and F was Faraday constant (96500 C mol^{-1}).

1.6.2 Determination of cathode products and calculation of FE.

Gas products from the cathodic compartment during CO_2RR were analyzed using a gas chromatography (GC online test, Agilent 8860) equipped with a thermal conductivity detector (TCD to H_2) and flame ionization detector (FID to CO). Ar was used as the carrier gas. When the mixed gas flow introduced into GC, 1 mL of gas was sampled to determine the concentration of gaseous products. The CO and H_2 Faradaic efficiencies were calculated based on:

For gaseous products, the FE was calculated as follows:

$$FE_{gas} = \frac{\frac{v \times 10^{-6} \times V}{V_m} \times n \times F}{Q} \times 100\ \%$$

v (ppm): volume concentration of certain gas product in the exhaust gas from the cathode compartment.

V: the gas volume in the cathode compartment.

n: the number of electrons transferred when one target gas molecule generated

Q: the total passed charge.

$V_m = 22.4\ L\ mol^{-1}$.

$F = 96500\ C\ mol^{-1}$.

The FE_{CO} and FE_{H2} were tested online and averaged for multiple data, and the error is less than 6%.

And the selectivity of CO was calculated as follows.

$$Selectivity_{gas} = \frac{FE_{gas}}{FE_{total}} \times 100\ \%$$

1.6.3 Determination of calculation of EE.

the full-cell EE is highly associated with the cell voltage and faradaic efficiency, as given by the equation：

$$EE = \frac{Energy\ required}{Enegy\ input} = \frac{\Delta G^{\theta}\mathrm{n}}{E_{cell}It} = \frac{zE^{\theta}Fn}{E_{cell}It} = \frac{E^{\theta}Q}{E_{cell}It}$$

For HMFOR-CO_2RR:

$$EE = \frac{E^{\theta} It}{E_{cell} It} FE = \frac{E^{\theta}}{E_{cell}} FE = \frac{E_{HMFOR} - E_{CO_2RR}}{E_{cell}} FE$$

For HMFOR-HER:

$$EE = \frac{E^{\theta} It}{E_{cell} It} FE = \frac{E^{\theta}}{E_{cell}} FE = \frac{E_{HMFOR} - E_{HER}}{E_{cell}} FE$$

ΔG^{θ}: the standard Gibbs free energy change,

n: the molar amount of the desired product,

E^{θ}: the thermodynamic potential of the overall reaction,

E_{HMFOR}= 0.3 V, E_{CO_2RR}= -0.11 V, E_{HER}= 0 V,

E_{cell}: actual applied potential,

F: the Faraday constant, 96500 C mol^{-1},

z is the electron transfer number,

Q: the amount of the Coulomb charge transferred into the desired product,

I: the total current,

t: the operation time,

FE: the faradaic efficiency

1.7. Theoretical calculation method:

The purpose of DFT calculation in this study is to reveal the intrinsic electronic structure difference between $NiCo_2O_4$ and Co_3O_4 catalysts and its influence on the intrinsic adsorption trend of reaction intermediates. Spin-polarized first-principle calculations were performed by the density functional theory (DFT) using the Vienna Ab-initio Simulation Package (VASP) package. The generalized gradient approximation (GGA) with the Perdew-Burke-Ernzerhof (PBE) functional were used to describe the electronic exchange and correlation effects with semi-empirical correction by Grimme (DFT+D3) included. Uniform G-centered k-points meshes with a resolution of $2\pi \times 0.05$ $Å^{-1}$ and Methfessel-Paxton electronic smearing were adopted for the integration in the Brillouin zone for geometric optimization. The simulation was run with a cutoff energy of 500 eV throughout the computations. The geometry optimization was considered convergent when the electronic energy and Hellmann-Feynman forces convergence criterion was smaller than 10^{-5} eV and 0.03 eV $Å^{-1}$, respectively. A vacuum distance of 15 Å was set to ensure sufficient vacuum and avoid interactions between two periods. The free energy was calculated using the equation: G= E + ZPE − TS, where G, E, ZPE, and TS were the free energy, total energy from DFT calculations, zero point energy, and entropic contributions (T was set to be 298.15 K), respectively. In order to obtain more accurate electronic properties, GGA+U method was applied with U-J values with 5.5 eV for Ni-3d and 3 eV for Co 3d electrons.

1.7.1. The calculated adsorption energy of HMF and OH on Co_3O_4 (111) and $NiCo_2O_4$ (111)

surfaces

The adsorption energy of HMF and OH on Co_3O_4 (111) and $NiCo_2O_4$ (111) surfaces was calculated by the following equation:

$\Delta E(ads)=E(total)-E(surface)-E(molecule)$

in which, E(total) represents the energy of HMF and OH adsorbed on Co_3O_4 (111) and $NiCo_2O_4$ (111) surfaces, E(surface) represents the energy of Co_3O_4 (111) and $NiCo_2O_4$ (111) surface, E(molecule) represents the energy of HMF and OH molecules. The calculated results are listed in **Table S1-2**.

1.7.2 Energy change of HMF oxidized to FDCA at Ni and Co sites of $NiCo_2O_4$ (111) surface

The catalytic process of from benzyl alcohol to benzoic acid at Ni and Co sites of NiCo2O4 (111) surface can be expressed as follows:

Path 1:

Step1: $* + C_6H_6O_3\ (g) \rightarrow C_6H_6O_3*$

Step2: $C_6H_6O_3* + 2OH^- \rightarrow C_6H_6O_4* + H_2O$

Step3: $C_6H_6O_4* + 2OH^- \rightarrow C_6H_4O_4* + 2H_2O$

Step4: $C_6H_4O_4* + 2OH^- \rightarrow C_6H_4O_5* + H_2O$

Step5: $C_6H_4O_5* \rightarrow * + C_6H_4O_5\ (g)$

Path 2:

Step1: $* + C_6H_6O_3\ (g) \rightarrow C_6H_6O_3*$

Step2: $C_6H_6O_3* + 2OH^- \rightarrow C_6H_4O_3* + 2H_2O$

Step3: $C_6H_4O_3* + 2OH^- \rightarrow C_6H_4O_4* + H_2O$

Step4: $C_6H_4O_4* + 2OH^- \rightarrow C_6H_4O_5* + H_2O$

Step5: $C_6H_4O_5* \rightarrow * + C_6H_4O_5\ (g)$

where* presents the $NiCo_2O_4$ (111) surface, and intermediates* denotes the corresponding absorbed intermediates.

2. Supplementary Figures

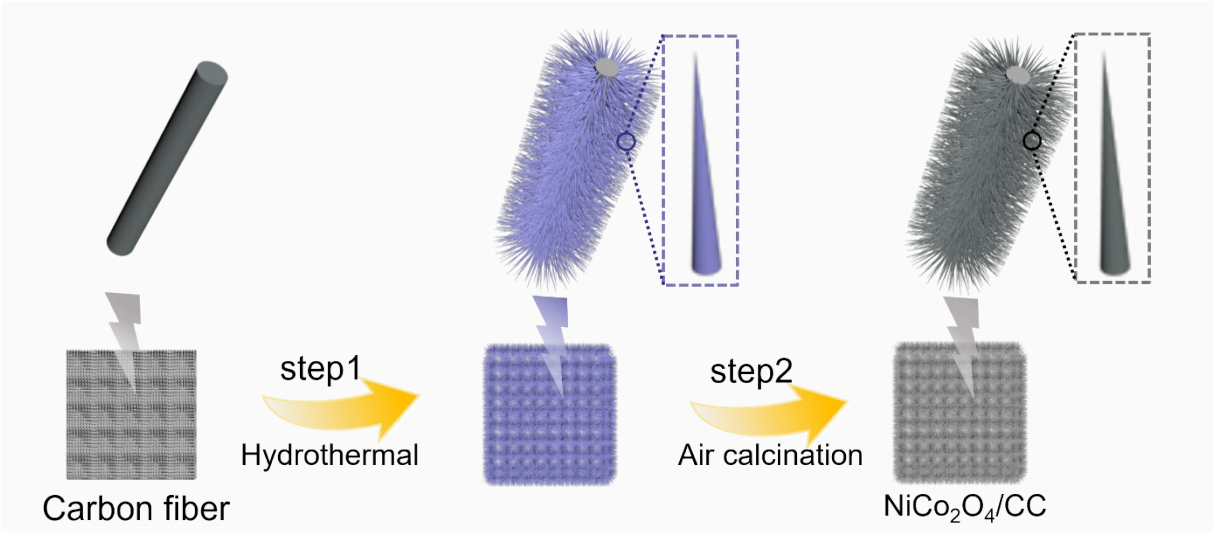

Figure S1. Synthetic processes of $NiCo_2O_4$.

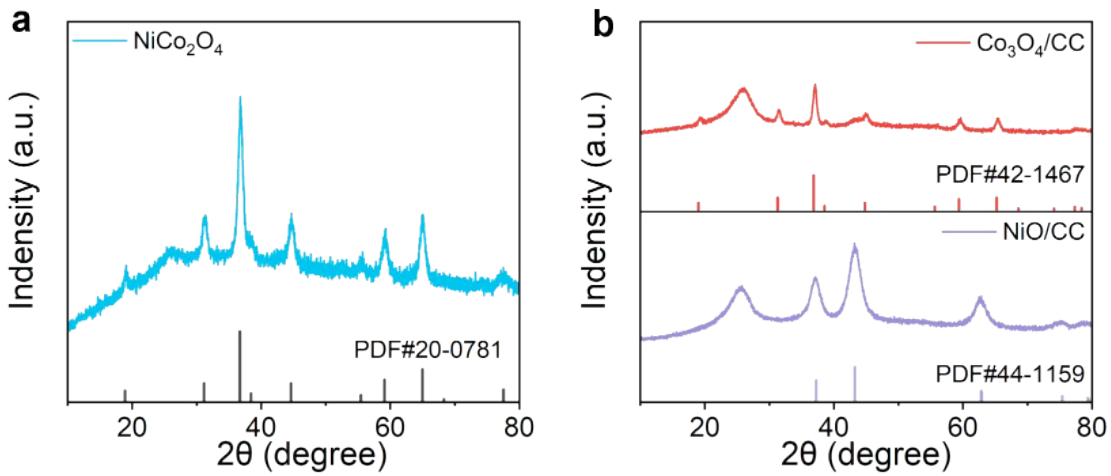

Figure S2. XRD of (a) $NiCo_2O_4$, (b) NiO and Co_3O_4.

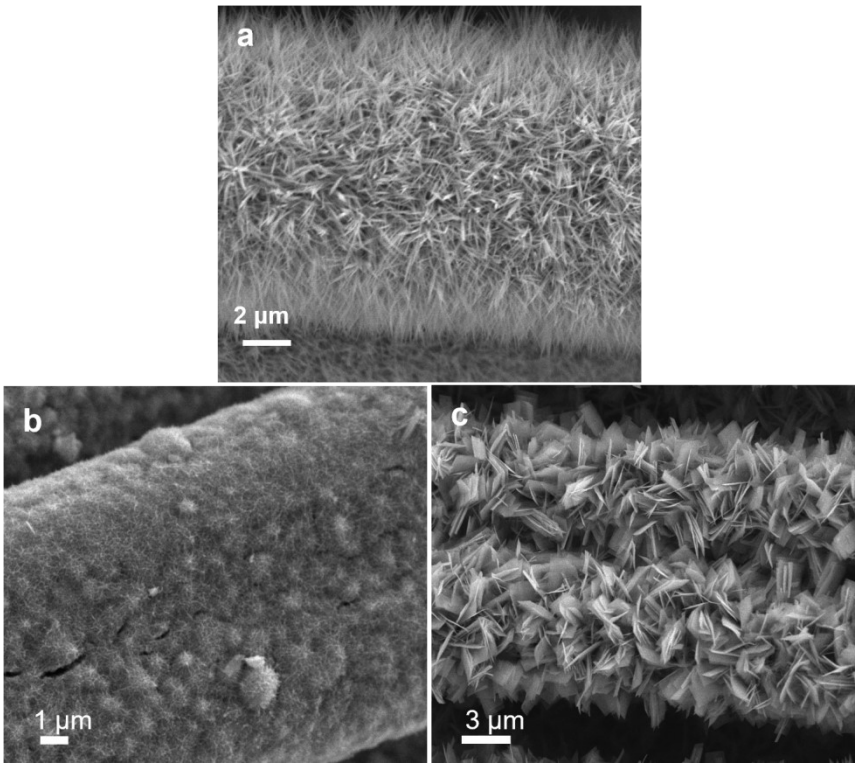

Figure S3. SEM images of (a) $NiCo_2O_4$ (b) NiO and (c) Co_3O_4.

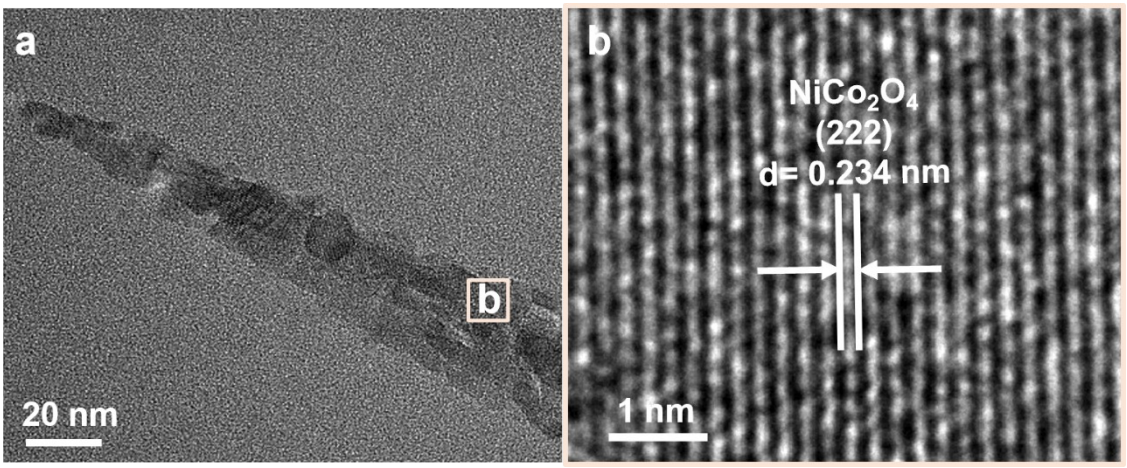

Figure S4. (a) TEM and (b) HRTEM of the $NiCo_2O_4$ samples.

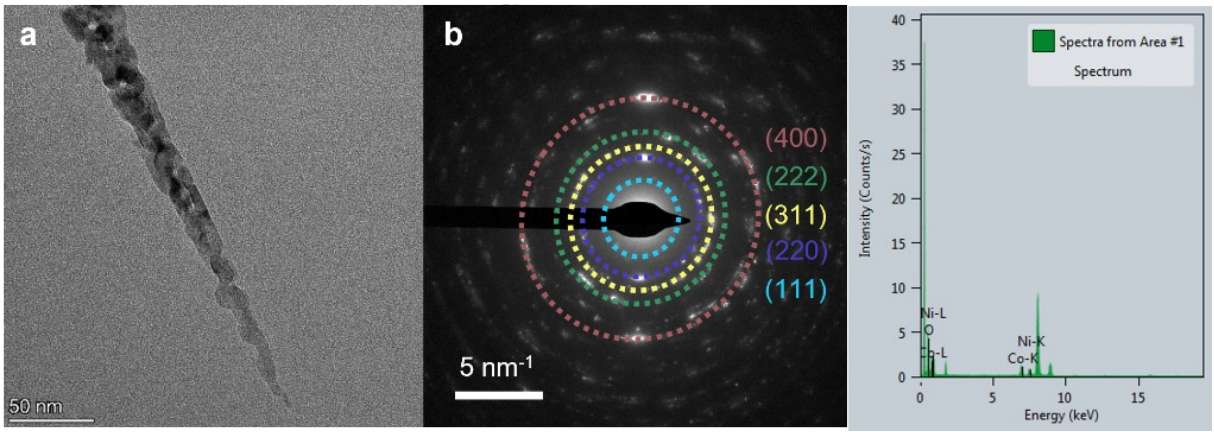

Figure S5. (a) The TEM images and (b) SAED of $NiCo_2O_4$.

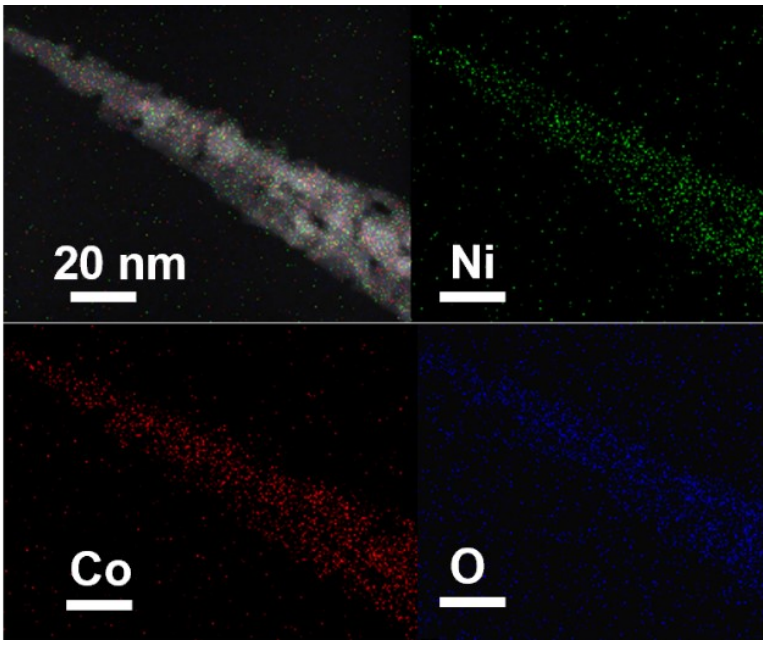

Figure S6. EDS mapping images of the $NiCo_2O_4$ sample.

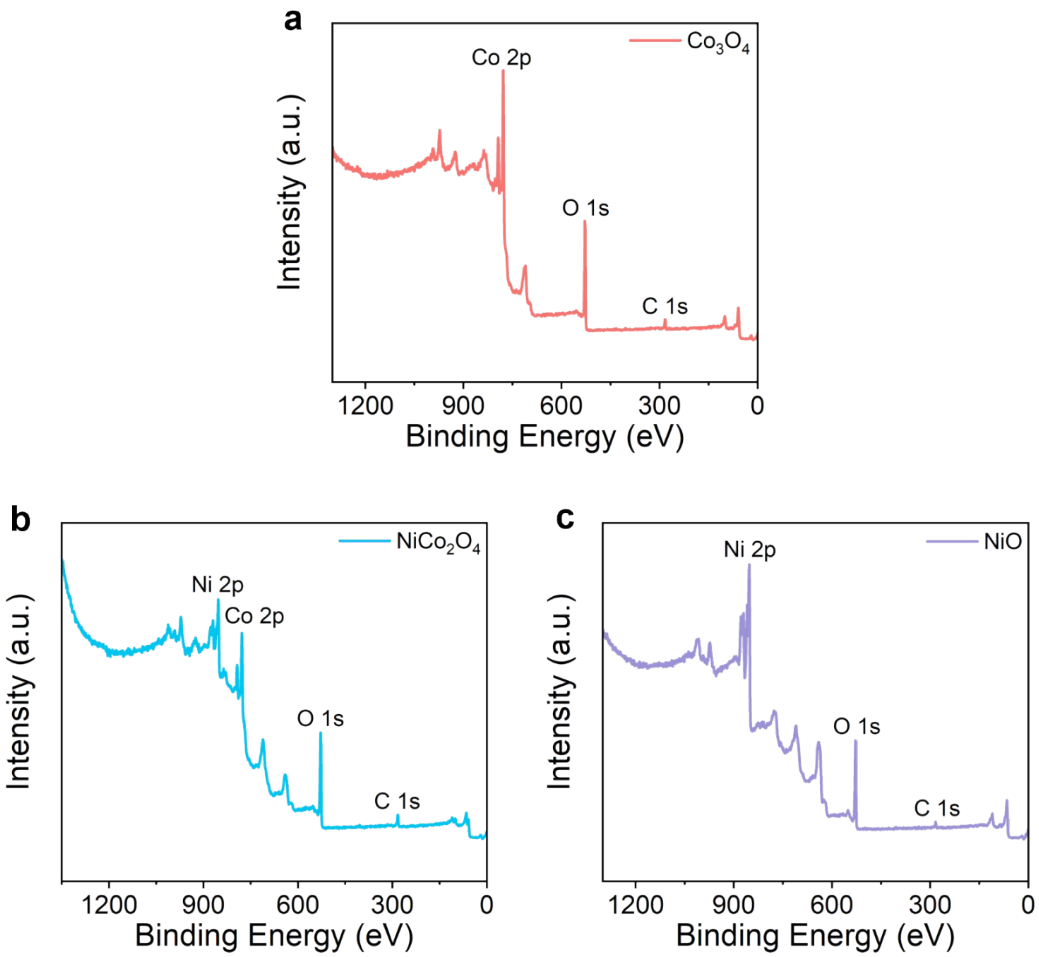

Figure S7. Full-scan XPS spectra of (a) Co_3O_4, (b) $NiCo_2O_4$ and (c) NiO.

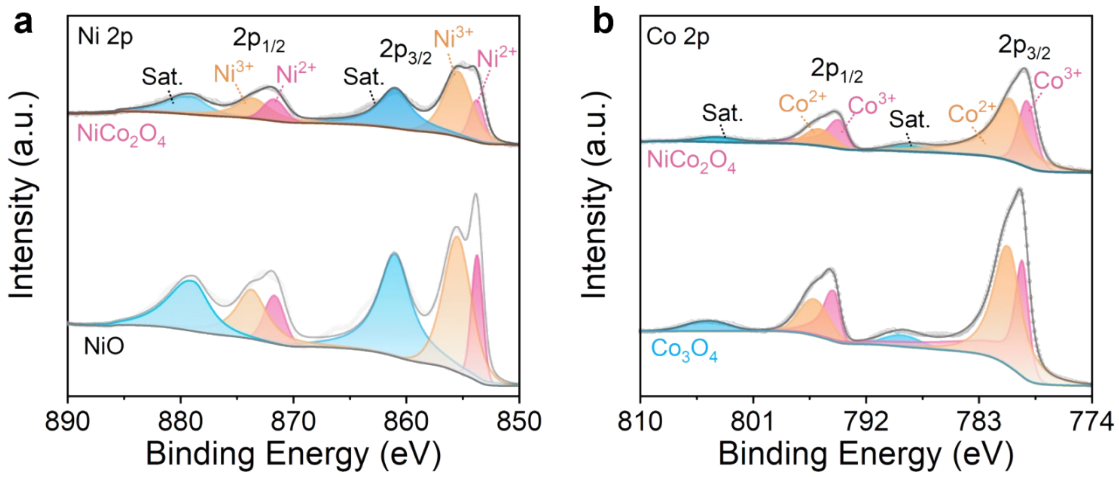

Figure S8. (a) High-resolution Ni 3d XPS spectra of $NiCo_2O_4$ and NiO. (b) High-resolution Co 2p XPS spectra of $NiCo_2O_4$ and Co_3O_4.

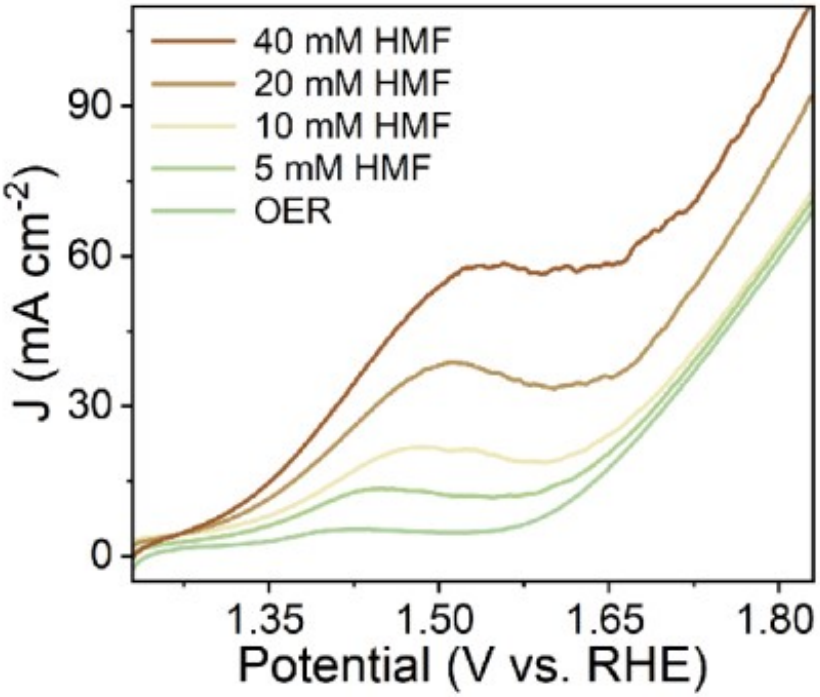

Figure S9. LSV of $NiCo_2O_4$ in 0, 5, 10,20, 40 mM HMF.

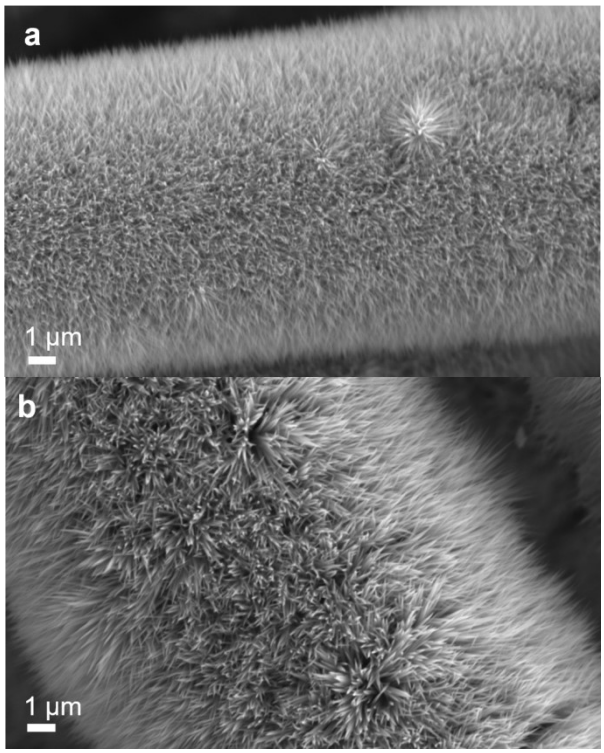

Figure S10. SEM of Ni Co with different feeding ratios：(a) 1:1, (b) 1:2.

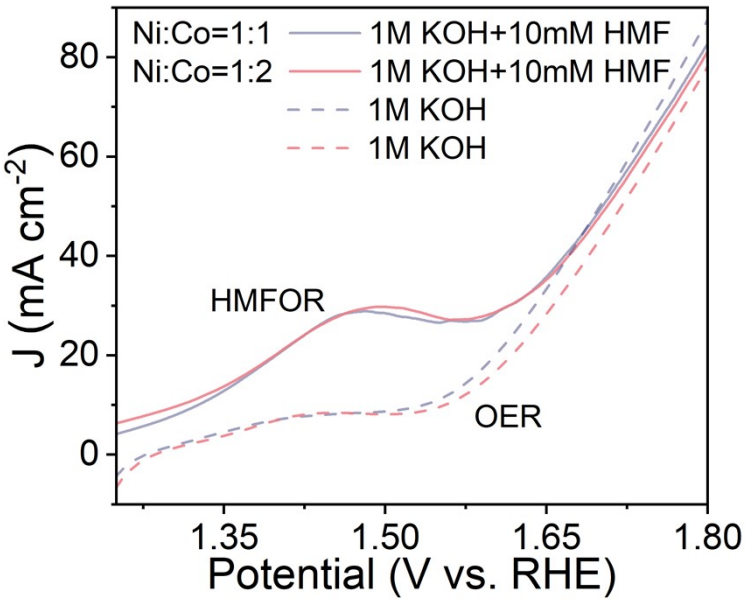

Figure S11. LSV of Ni Co with different feeding ratios: 1: 1 and 1: 2.

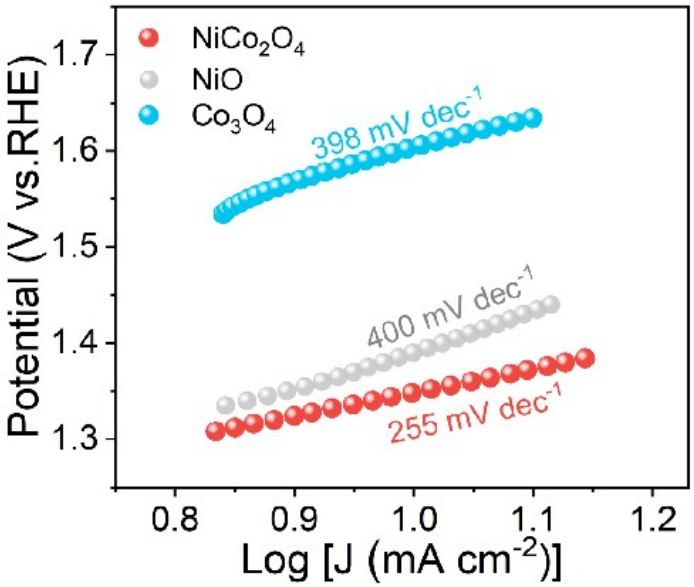

Figure S12. Tafel of NiO, Co_3O_4 and $NiCo_2O_4$ for HMFOR in 10 mM HMF + 1 M KOH solution.

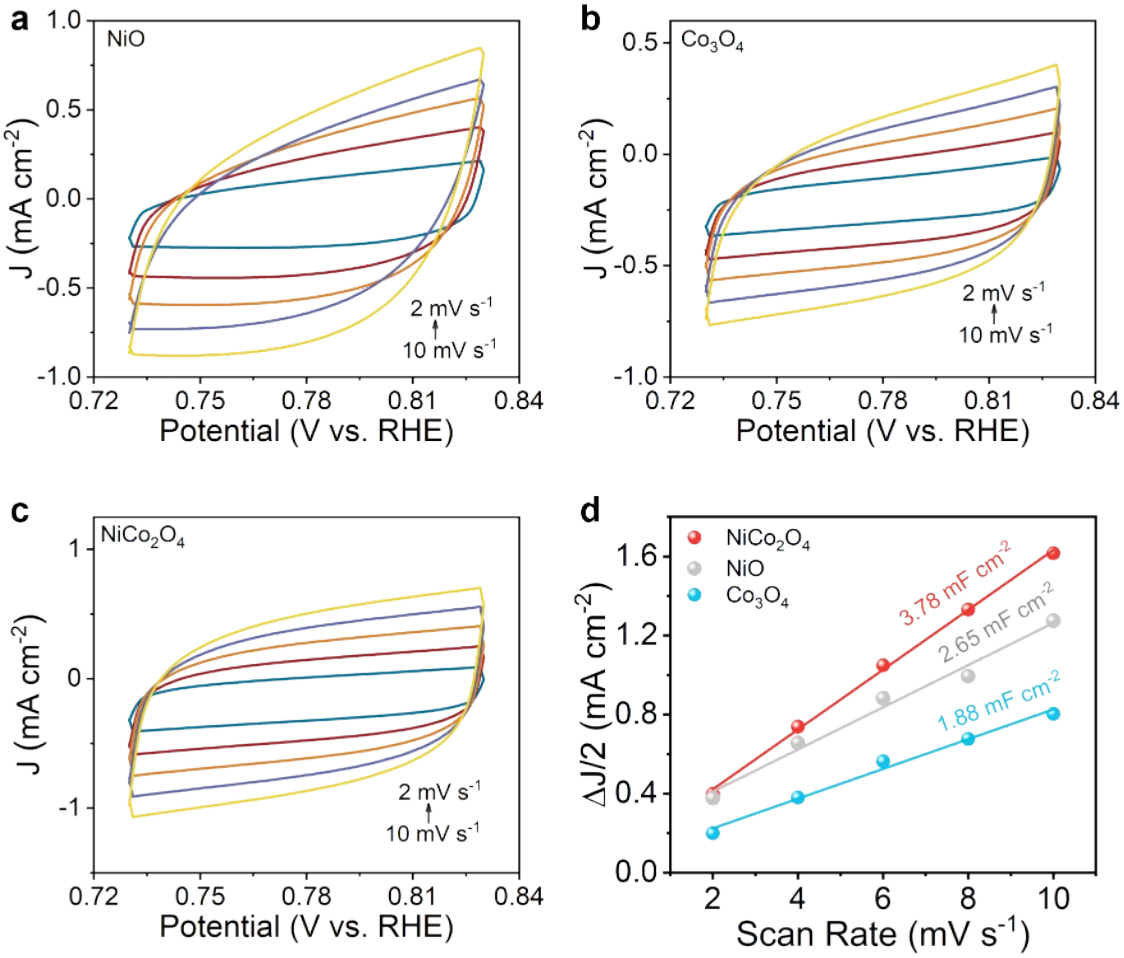

Figure S13. ECSA spectra of the (a) NiO, (b) Co_3O_4 and (c) $NiCo_2O_4$ samples. (d) Electric double layer capacitor (EDLC) spectrum of the NiO, Co_3O_4 and $NiCo_2O_4$ samples.

Name	Formula	Annot. DeltaMass [Da]	Annot. DeltaMass [ppm]	Annotation MW	Calc. MW	RT [min]	# ChemSpider Results	# mzCloud Results	# mzVault Results	mzCloud Best Match	mzVault Best Match	MS2	Area: blk2.raw (F3)	Area: hou.raw (F4)
Sulfuric acid	H2 O4 S	-0.00006	-0.64	97.96738	97.96732	0.869	1	0	0			DDA for other ion		16118774908
Palmitic Acid	C16 H32O2	17.02602	66445.53	256.24023	273.26625	14.174	8	1	2	80.9	61.6	DDA for preferred ion		1756836277
5-Hydroxymethyl-2-furaldehyde	C6 H6O3	-0.00016	-1.26	126.03169	126.03154	2.482	20	0	0			DDA for preferred ion		777805419.8
2,5-Furandicarboxylic acid	C6 H4O5	-0.00015	-0.95	156.00587	156.00573	2.201	100	5	16	99	90.3	DDA for preferred ion		1110452783
1,8,15,22,29,36-Hexaazacyclodotetracontane-2,9,16,23,30,37-hexone	C36 H66 N6 O6	-0.00136	-2.01	678.50438	678.50302	11.901	2	0	0			DDA for other ion		758114522
tetraethynylethene	C10 H4	0.00022	1.76	124.0313	124.03152	0.683	2	0	0			DDA for preferred ion		735717910.6

Figure S14. HPLC - MS of the $NiCo_2O_4$ sample at 1.5 V *vs*. RHE in the process of HMFOR.

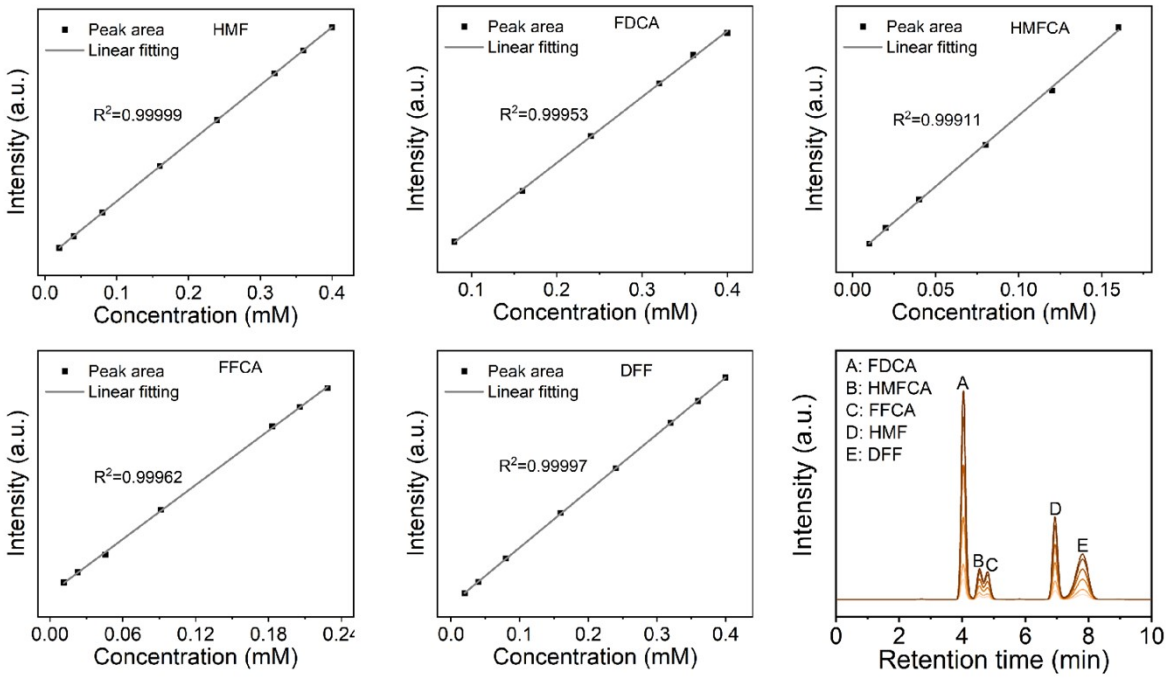

Figure S15. HPLC standard curves of the HMF, HMFCA, FFCA, FDCA and DFF.

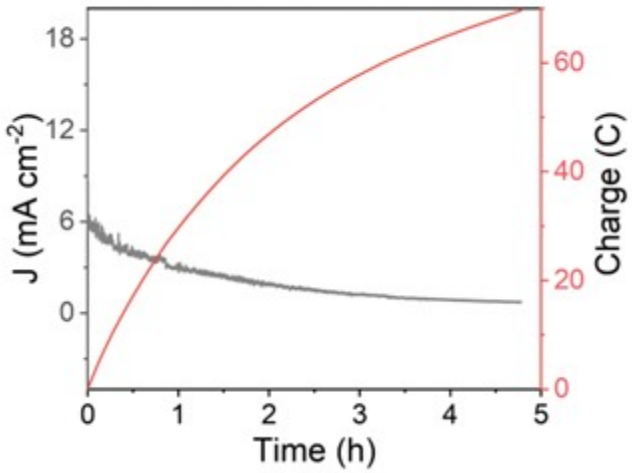

Figure S16. The i-t curves and charge amount of $NiCo_2O_4$ sample in in the electrolysis process.

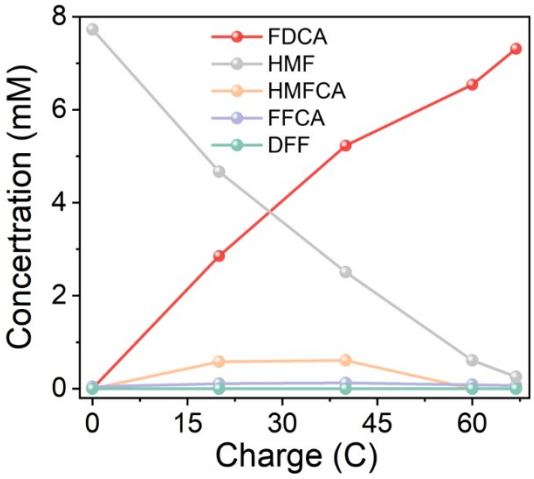

Figure S17. Concentration of HMF and its oxidation products under different charges on $NiCo_2O_4$ at 1.50 V *vs*. RHE in 10 mM HMF.

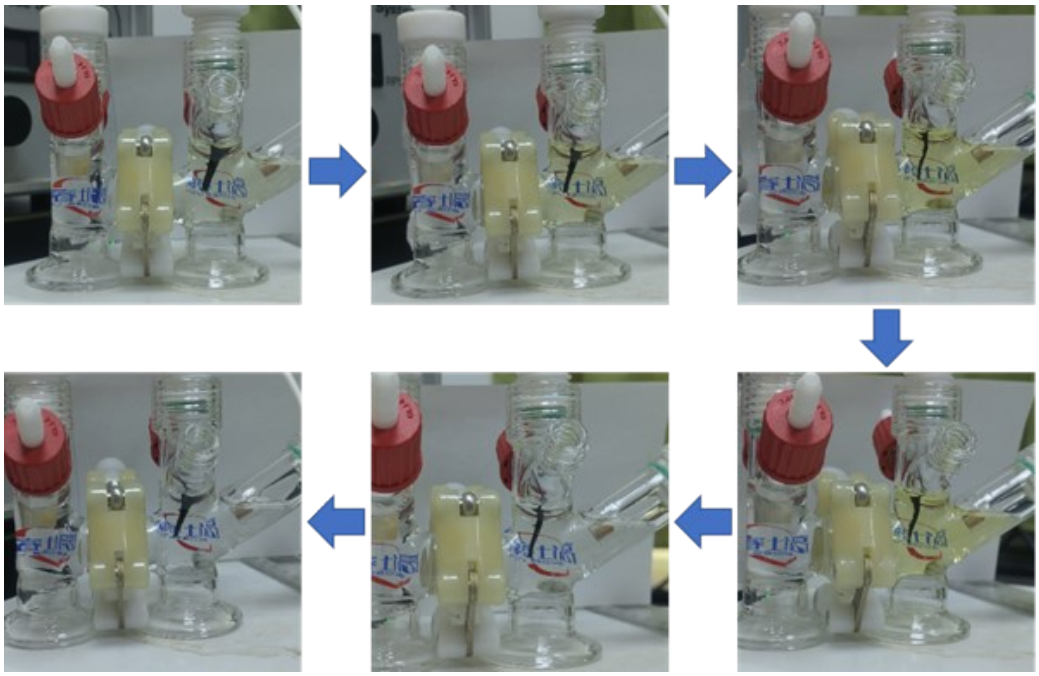

Figure S18. The color change of the reaction solution during the specific experiment.

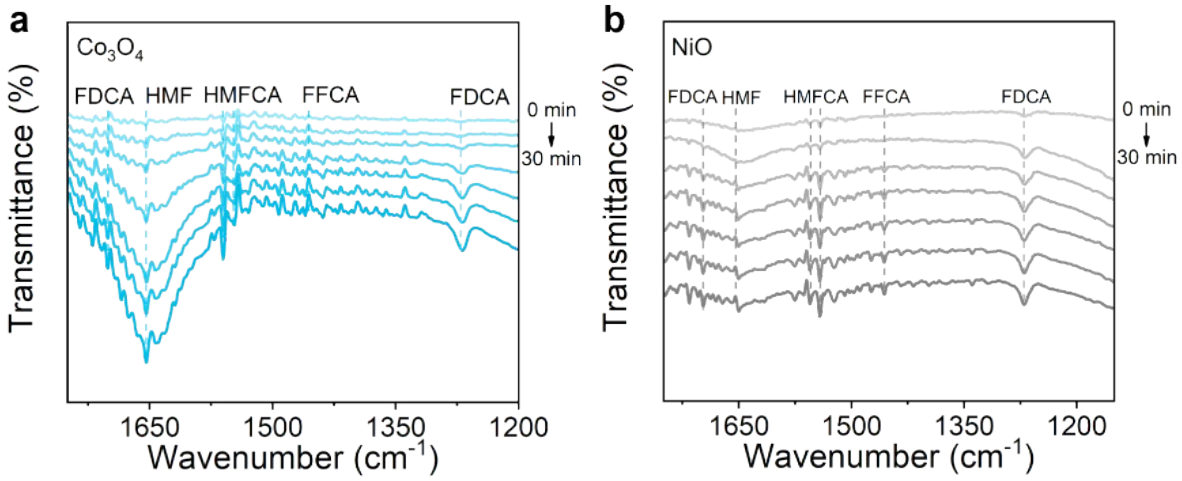

Figure S19. In situ-FTIR spectra of (a) Co_3O_4 and (b) NiO samples.

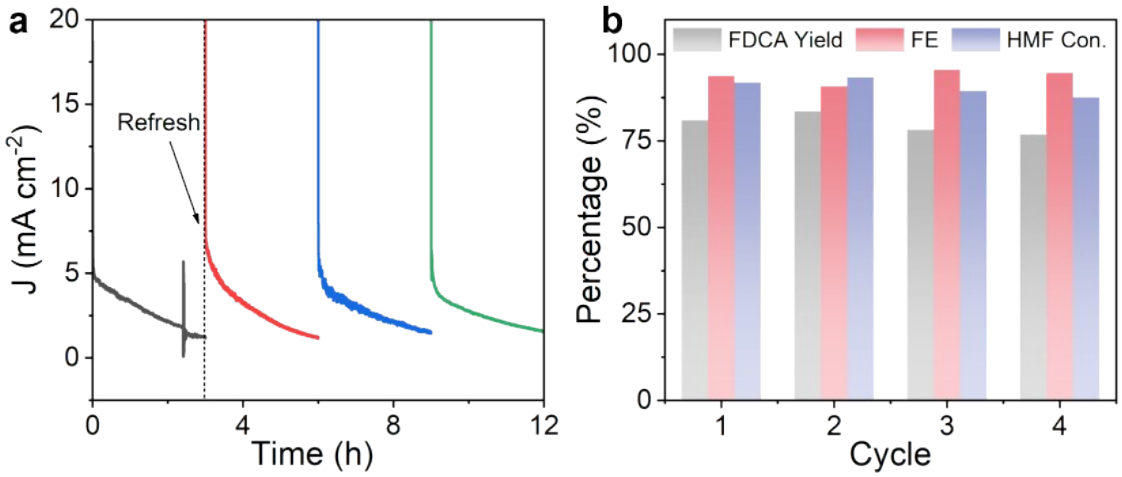

Figure S20. (a) The i-t cycle curves of the $NiCo_2O_4$ sample at 1.5 V *vs*. RHE in the process of HMFOR. (b) Reusable HMFOR tests under 4 successive cycles over $NiCo_2O_4$.

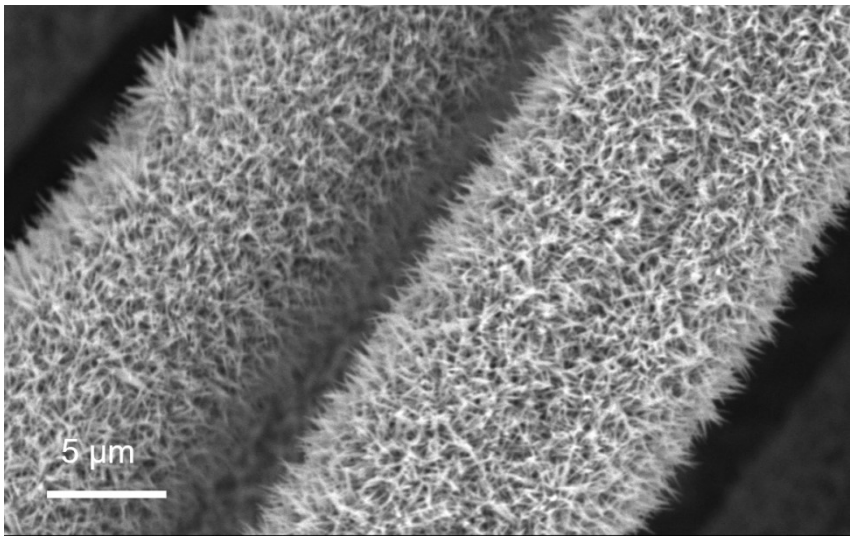

Figure S21. SEM image of $NiCo_2O_4$ after electrochemical oxidation.

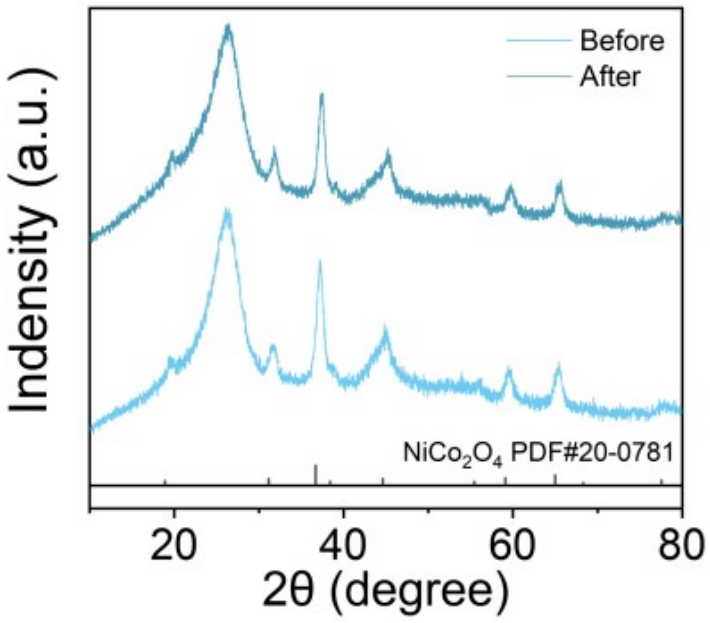

Figure S22. XRD patterns of $NiCo_2O_4$ before and after HMFOR cycling stability.

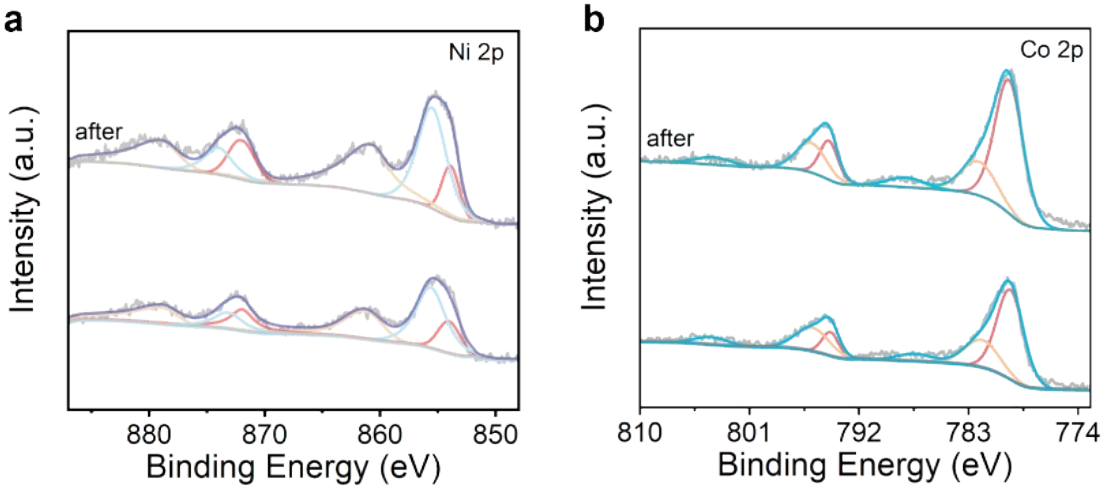

Figure S23. (a) Ni 2p and (b) Co 2p XPS spectra of the $NiCo_2O_4$ sample before and after electrolysis.

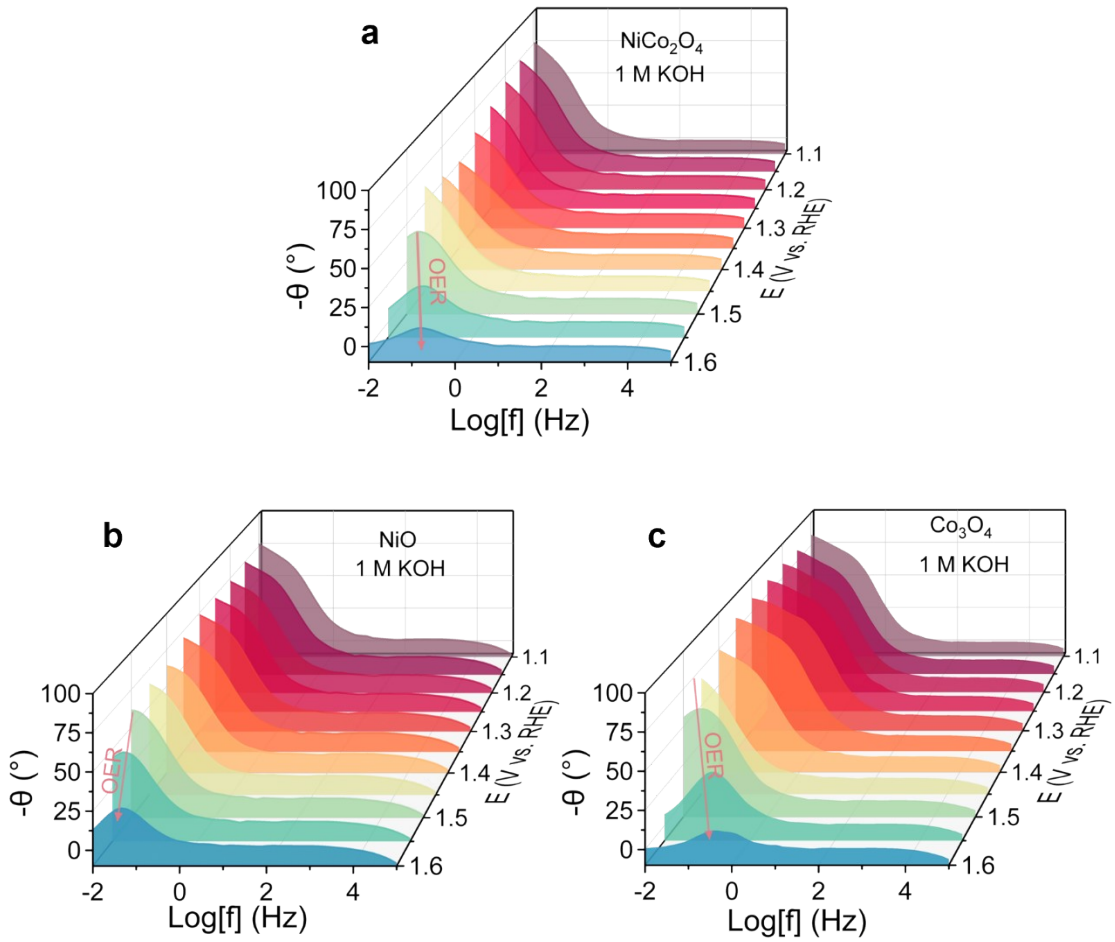

Figure S24. Bode phase plots of the in-situ EIS on (a) $NiCo_2O_4$, (b) Co_3O_4 and (c) NiO in 1 M KOH.

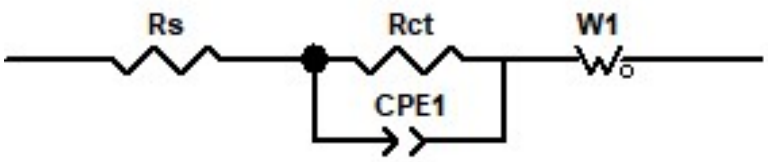

Figure S25. Based on the Bode diagram data, the EIS fitting equivalent circuit diagram of Co_3O_4 $NiCo_2O_4$ and NiO samples.

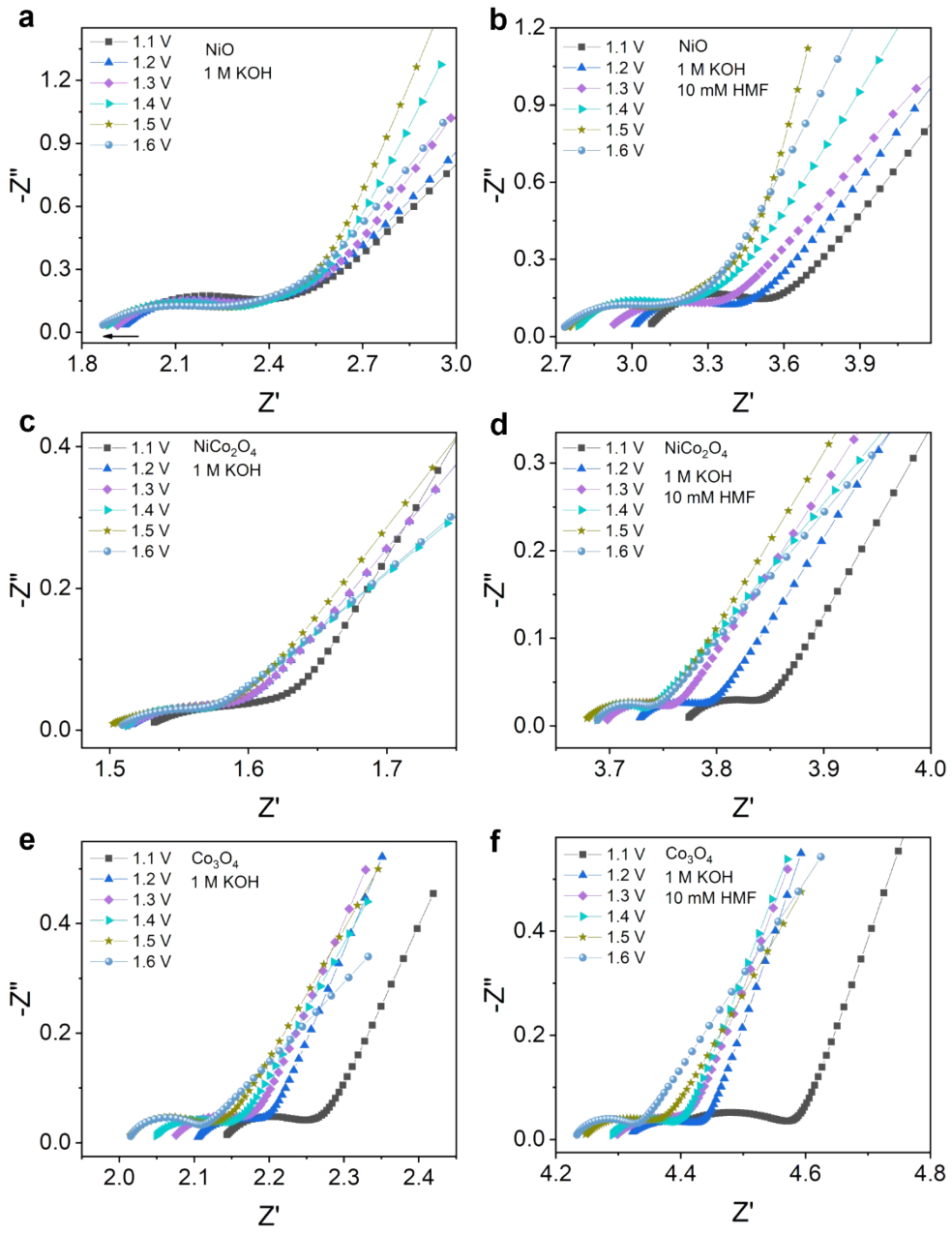

Figure S26. The EIS Nyquist plots of the Co_3O_4 $NiCo_2O_4$ and NiO samples for (a, c, e) 1 M KOH and (b, d, f) 1 M KOH + 10 mM HMF.

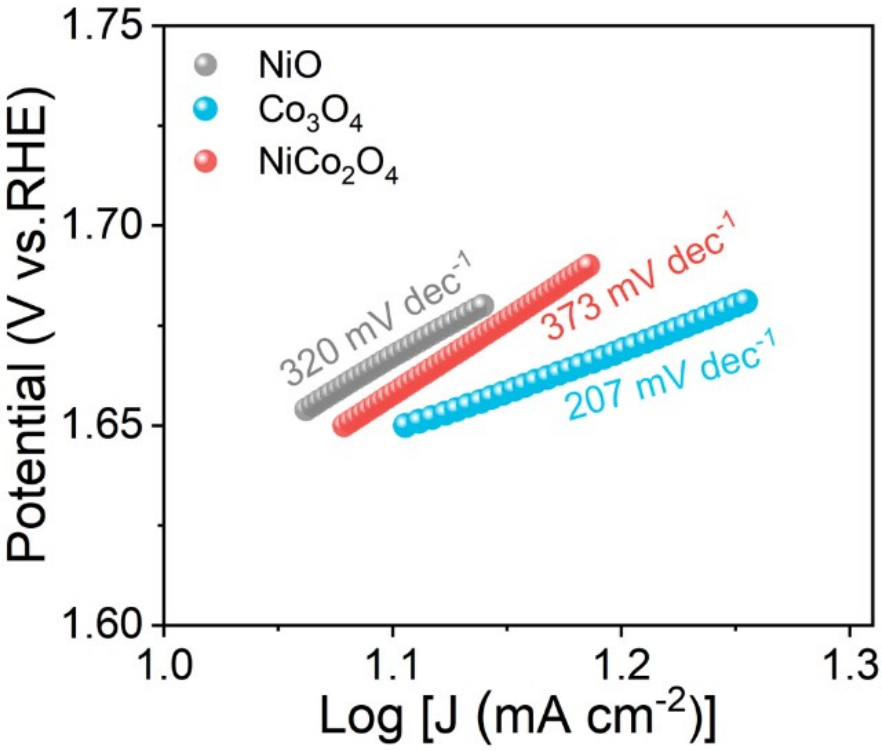

Figure S27. The Tafel slope values of the three samples for OER in 1 M KOH solution.

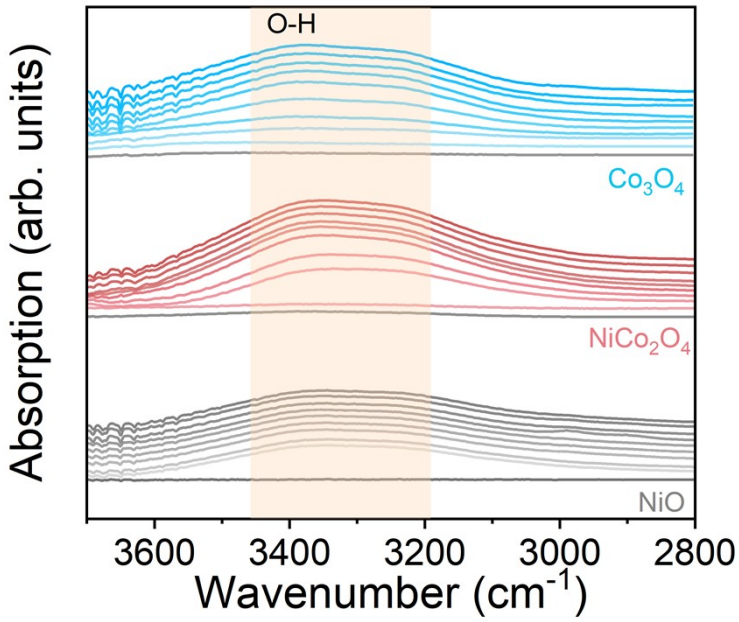

Figure S28. From the bottom to the top, the first six wires were used to detect the in-situ FTIR changes of O-H in Co_3O_4 $NiCo_2O_4$ and NiO within 0 − 30 min, and the last four wires were used to monitor the infrared data every 5 min after the end of electrification for 20 min.

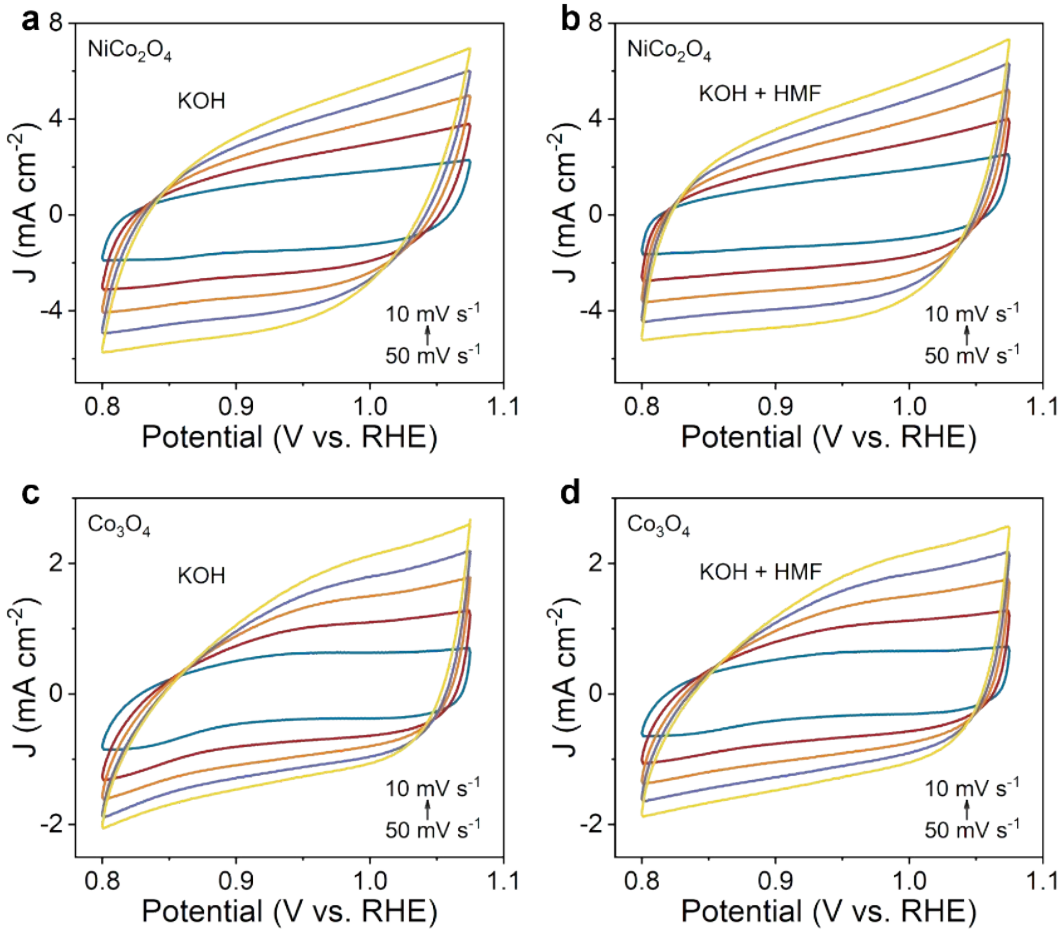

Figure S29. The CV curves of the Co_3O_4 and $NiCo_2O_4$ samples in (a, c) 1 M KOH or (b, d)1 M KOH + 10 mM HMF solution in the potential range of 0.8 V − 1.05 V *vs*. RHE.

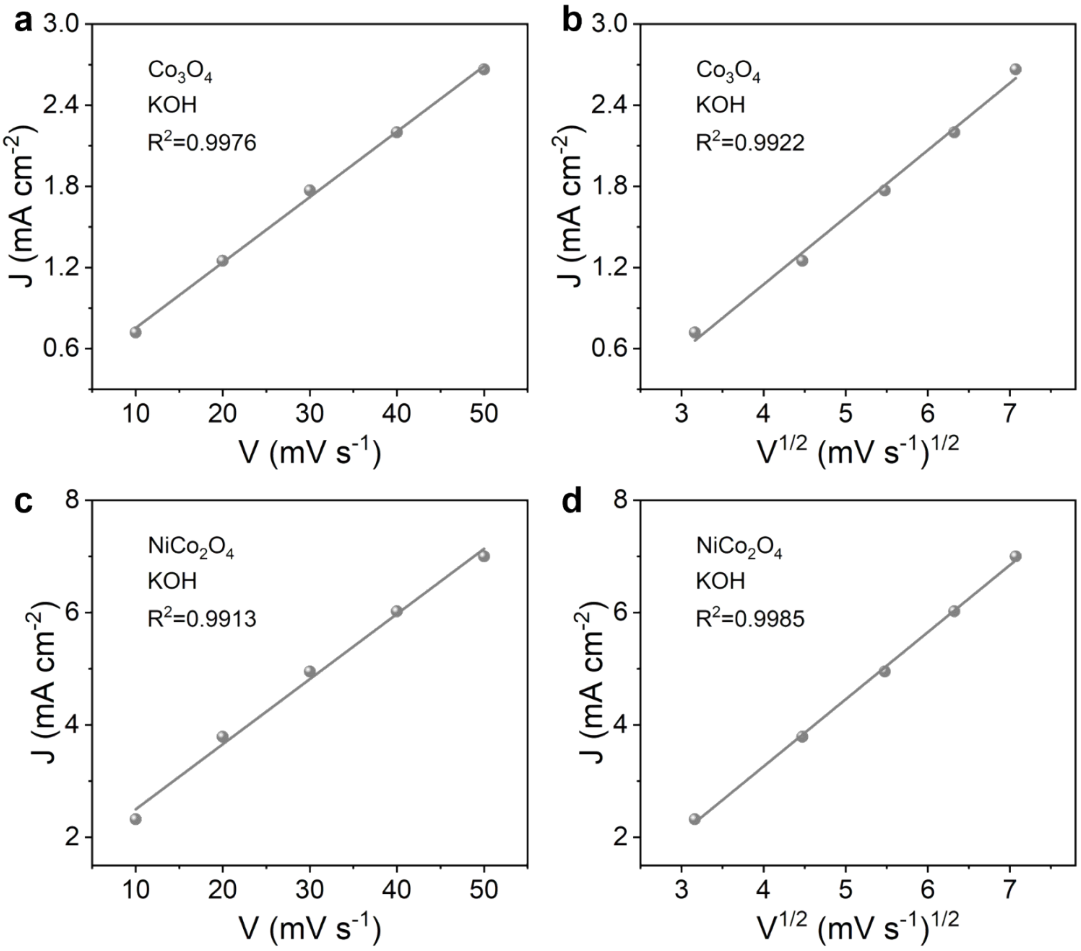

Figure S30. The linear relation of peak current (j) and (a, c) sweep speed (v) or (b, d) sweep speed square ($v^{1/2}$) for Co_3O_4 and $NiCo_2O_4$ in KOH solution.

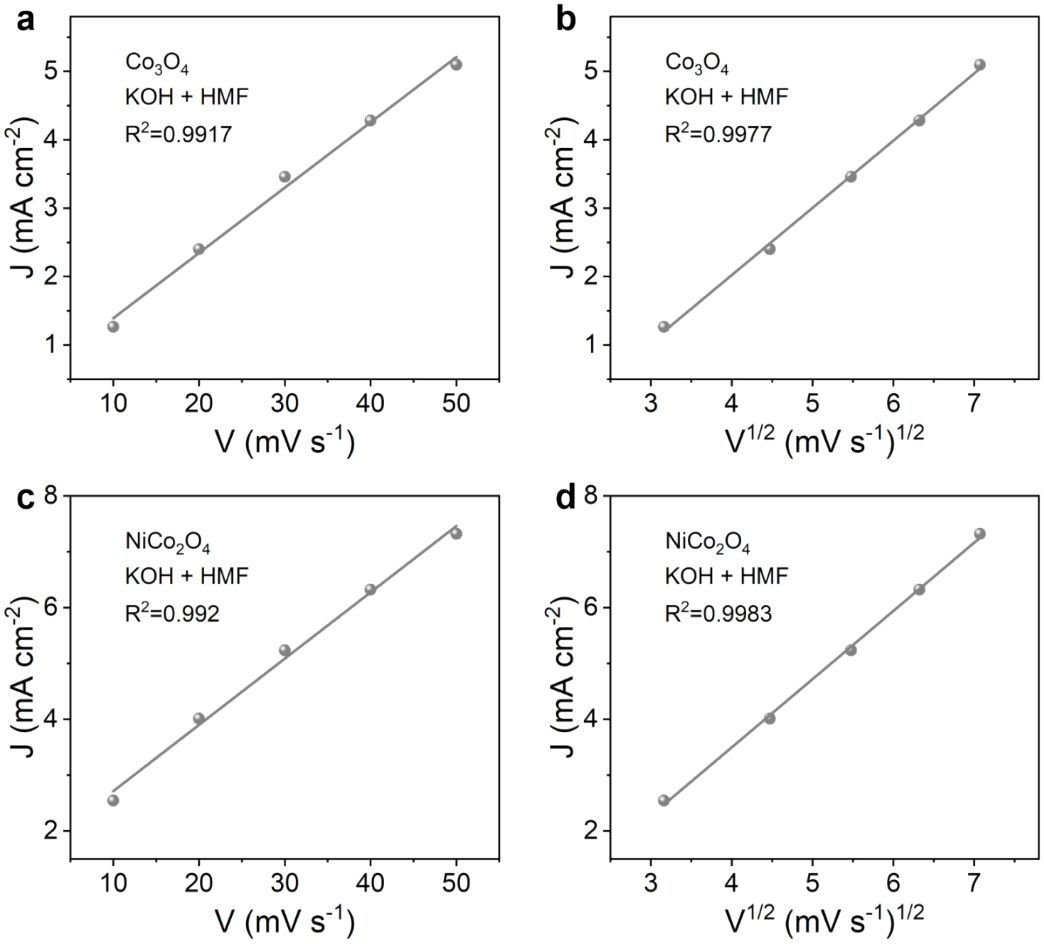

Figure S31. The linear relation of peak current (j) and (a, c) sweep speed (v) or (b, d) sweep speed square ($v^{1/2}$) for Co_3O_4 and $NiCo_2O_4$ in KOH + HMF solution.

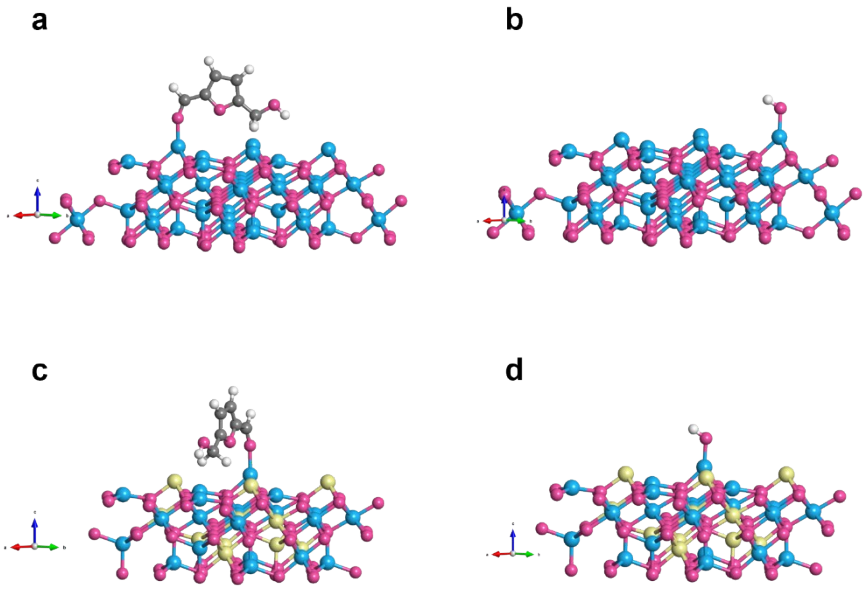

Figure S32. The optimized structures of HMF and OH adsorbed on (a, b) Co_3O_4 (111) and (b, d) $NiCo_2O_4$ (111) surfaces.

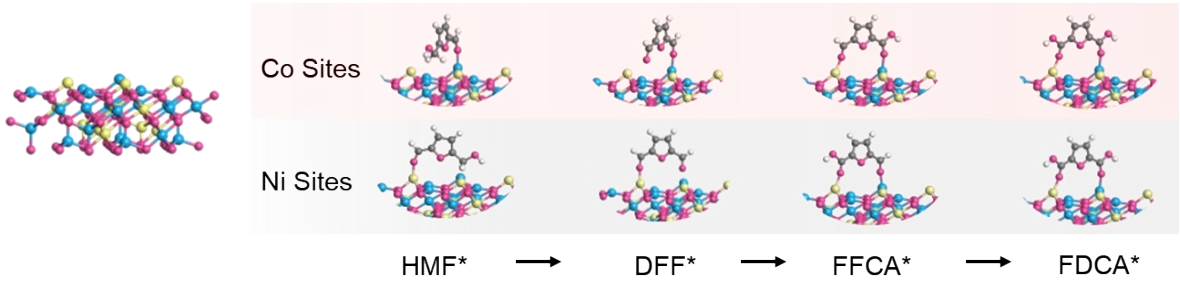

Figure S33. The adsorption configurations of HMFOR intermediate DFF on Ni sites and Co sites of $NiCo_2O_4$ and Co sites of Co_3O_4.

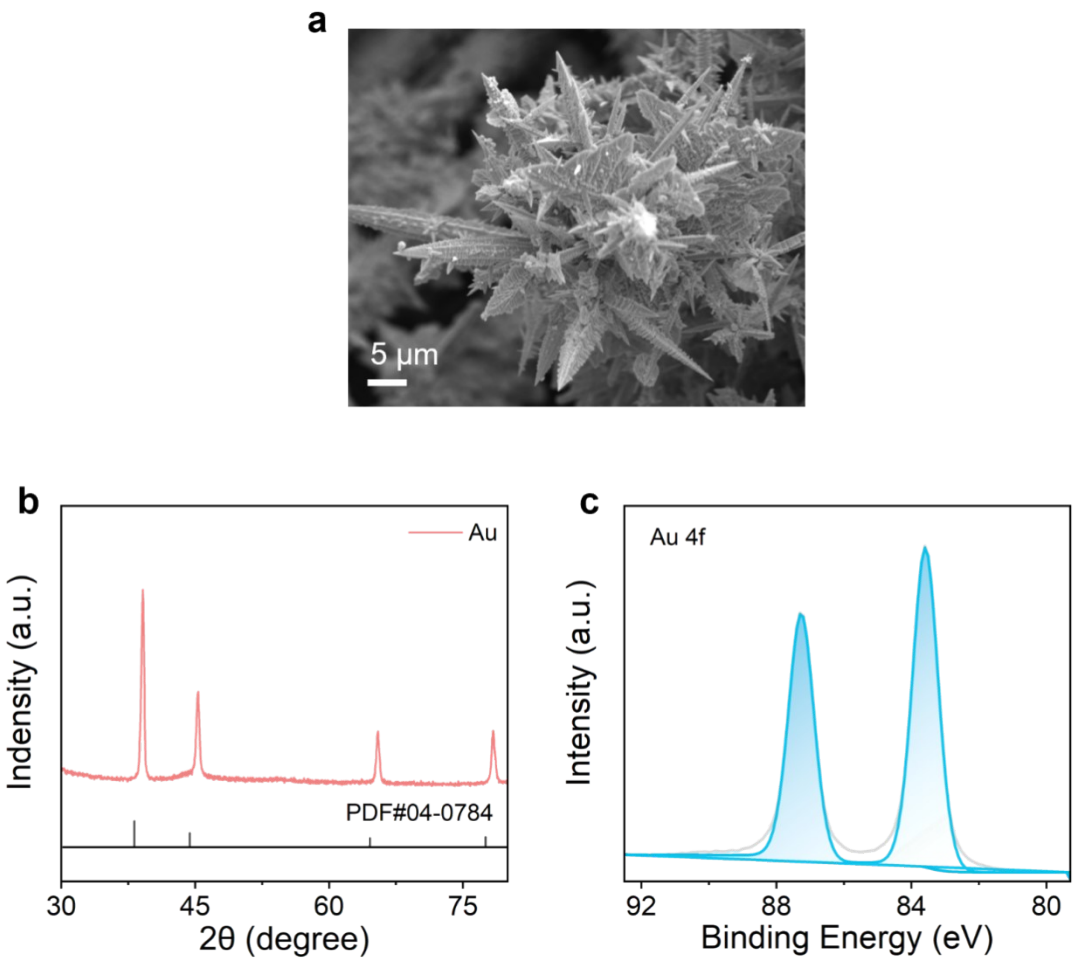

Figure S34. (a) SEM, (b) XRD and (c) XPS image of Au sample.

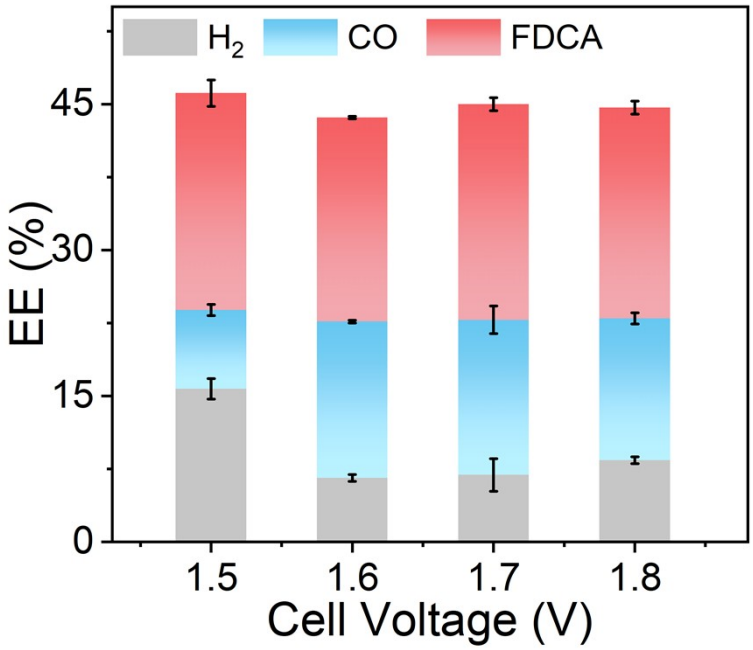

Figure S35. CO_2RR-HMFOR: FE and EE of CO and H_2 at different cell voltages.

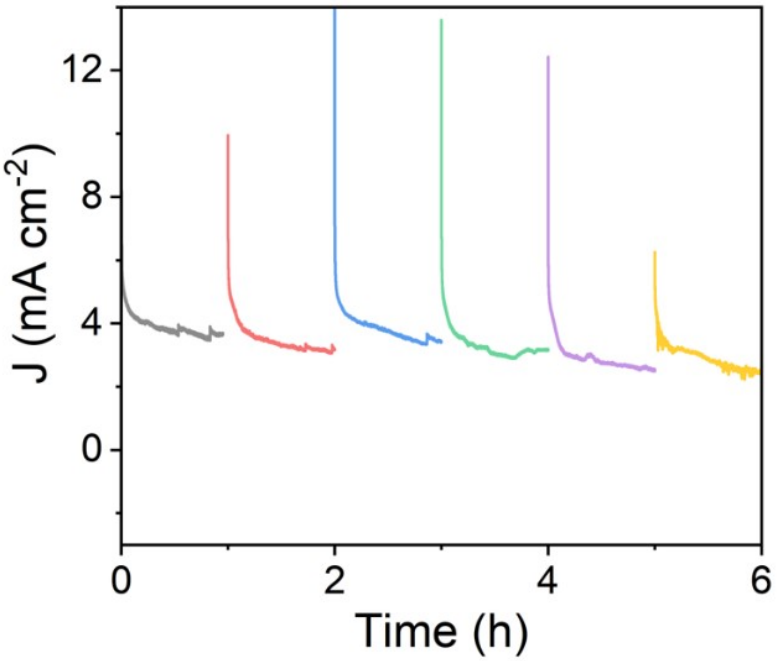

Figure S36. The stability of the CO_2RR-HMFOR coupling reaction was tested at a cell voltage of 1.70 V.

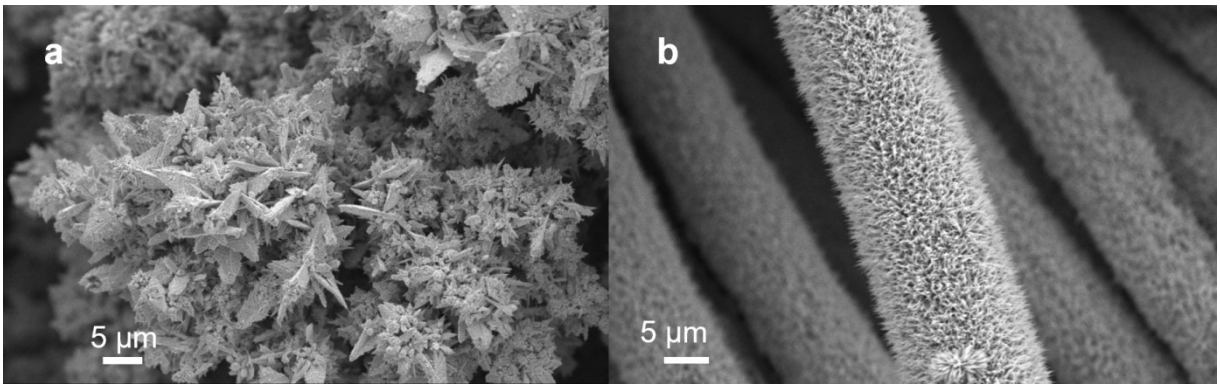

Figure S37. SEM image of (a) Au and (b) $NiCo_2O_4$ after CO_2RR-HMFOR cycle stability.

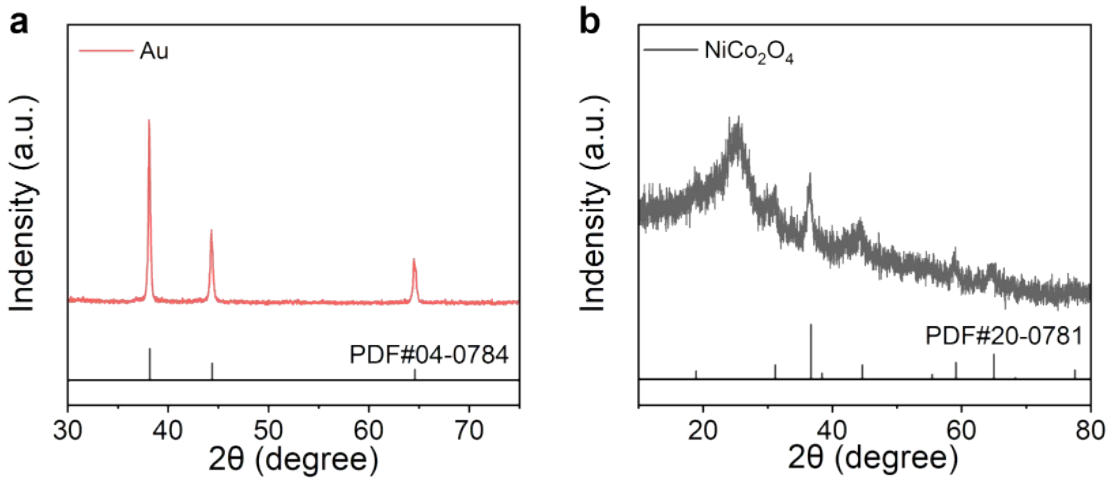

Figure S38. XRD image of (a) Au and (b) $NiCo_2O_4$ after CO_2RR-HMFOR cycle stability.

3. Supplementary Tables

Table S1. The equation of HMFOR two paths transformation and functional group transformation.

HMFCA path	**reaction equation**	**Functional groups changes**
1HMF → HMFCA	$C_6H_6O_3+H_2O \rightarrow C_6H_4O_3(DFF)+4H^++2e^-$	$-CH_2OH \rightarrow -CHO$
2 HMFCA → FFCA	$C_6H_4O_3(DFF)+H_2O \rightarrow C_6H_4O_4(FFCA)+4H^++2e^-$	-CHO → -COOH
3 FFCA → FDCA	$C_6H_4O_4(FFCA)+H_2O \rightarrow C_6H_4O_5(FFCA)+4H^++2e^-$	-CHO → -COOH
DFF path		
1 HM F→ DFF	$C_6H_6O_3+H_2O \rightarrow C_6H_4O_3(DFF)+4H^++2e^-$	$-CH_2OH \rightarrow -CHO$
2 DFF → FFCA	$C_6H_4O_3(DFF)+H_2O \rightarrow C_6H_4O_4(FFCA)+4H^++2e^-$	-CHO → -COOH
3 FFCA → FDCA	$C_6H_4O_4(FFCA)+H_2O \rightarrow C_6H_4O_5(FFCA)+4H^++2e^-$	-CHO → -COOH

Table S2. The related EIS fitting parameters of Co_3O_4 sample for OER.

Potential (V)	Rs	Rct	CPE1-T	CPE1-P	W1-R	W1-T	W1-P
1.1	2.134	0.079886	0.0027128	0.8907	0.16357	0.010774	0.39725
1.15	2.115	0.10172	0.010199	0.76865	0.00011927	1.3022E-6	0.39936
1.2	2.095	0.041854	0.0027737	1.003	0.17311	0.0095949	0.39915
1.25	2.078	0.046346	0.00203	1.038	0.18092	0.0077846	0.41788
1.3	2.064	0.055173	0.0035431	0.95532	0.17394	0.0073434	0.40531
1.35	2.053	0.122	0.013686	0.75522	9.6263E-5	1.5576E-6	0.41639
1.4	2.043	0.11119	0.016495	0.75588	0.00028431	5.9005E-6	0.37773
1.45	2.018	0.061537	0.0044607	0.95088	0.29651	0.17209	0.35473
1.5	2.006	0.076364	0.0037006	0.94055	0.1751	0.043092	0.37525
1.55	2.011	0.10484	0.0068501	0.83516	0.00015735	2.0843E-6	0.3639
1.6	2.012	0.087649	0.0029502	0.93738	0.0004478	1.7162E-6	0.30862

Table S3. The related EIS fitting parameters of Co_3O_4 sample for HMFOR.

Potential (V)	Rs	Rct	CPE1-T	CPE1-P	W1-R	W1-T	W1-P
1.1	4.363	0.23042	0.011739	0.52996	0.0022513	4.9695E-5	0.41168
1.15	4.229	0.18725	0.031066	0.55925	0.010064	0.00021467	0.38159
1.2	4.309	0.13553	0.01966	0.57599	9.6788E-5	9.818E-7	0.41475
1.25	4.299	0.13497	0.041895	0.55519	0.00013938	9.4207E-7	0.39434
1.3	4.292	0.12464	0.019288	0.65395	0.00013316	1.0311E-6	0.40639
1.35	4.286	0.13285	0.026343	0.63175	9.633E-5	9.9544E-7	0.40497
1.4	4.285	0.11424	0.016125	0.71283	0.0088829	0.00052253	0.40334
1.45	4.271	0.090053	0.017477	0.75182	0.027999	0.0018345	0.32488
1.5	4.241	0.13042	0.03224	0.65355	0.0002765	5.4165E-6	0.36005
1.55	4.216	0.11616	0.011571	0.72772	0.00029063	4.2653E-6	0.36464
1.6	4.23	0.096047	0.80899	0.00065151	0.00065151	5.4229E-6	0.33962

Table S4. The related EIS fitting parameters of $NiCo_2O_4$ sample for OER.

Potential (V)	Rs	Rct	CPE1-T	CPE1-P	W1-R	W1-T	W1-P
1.1	1.522	0.049416	0.053801	0.71513	0.17855	0.035614	0.40886
1.15	1.525	0.092603	0.049337	0.70595	0.00024012	9.1937E-6	0.40522
1.2	1.51	0.085944	0.068783	0.68686	0.00043994	1.3908E-5	0.37506
1.25	1.509	0.046779	0.06724	0.71945	0.16335	0.044812	0.39962
1.3	1.509	0.087115	0.066514	0.68701	0.00012829	2.6833E-6	0.37498
1.35	1.51	0.053053	0.013231	0.87476	0.00058983	5.0325E-6	0.3315
1.4	1.51	0.054719	0.017293	0.8596	0.0005827	4.9671E-6	0.32521
1.45	1.501	0.088385	0.10159	0.63269	0.00014564	2.188E-6	0.35489
1.5	1.494	0.09483	0.13265	0.60344	0.01493	0.0022233	0.0022233
1.55	1.502	0.077478	0.056532	0.7208	0.0002582	9.473E-6	0.378
1.6	1.505	0.063132	0.048573	0.74378	0.00046375	5.7042E-6	0.32967

Table S5. The related EIS fitting parameters of $NiCo_2O_4$ sample for HMFOR.

Potential (V)	Rs	Rct	CPE1-T	CPE1-P	W1-R	W1-T	W1-P
1.1	3.768	0.075278	0.017849	0.74455	0.00025875	2.5815E-6	0.36276
1.15	3.749	0.061386	0.010266	0.81456	0.00042796	3.7546E-6	0.34545
1.2	3.723	0.067967	0.021944	0.73873	0.00039692	5.3761E-6	0.34927
1.25	3.704	0.066638	0.019912	0.76914	0.00032391	6.4318E-6	0.35161
1.3	3.694	0.062639	0.017949	0.77655	0.00047373	7.2627E-6	0.34631
1.35	3.693	0.059789	0.014972	0.80535	0.0010616	1.1844E-5	0.33113
1.4	3.686	0.043597	0.0048286	0.92897	0.00099596	6.9506E-6	0.31193
1.45	3.676	0.060061	0.020553	0.75781	0.00015445	1.0474E-6	0.33659
1.5	3.673	0.073473	0.035172	0.70602	0.0005249	1.0806E-5	0.35407
1.55	3.68	0.054123	0.0091034	0.8674	0.00031196	2.9193E-6	0.33736
1.6	3.686	0.047333	0.0073318	0.89668	2.208	1.907	0.61835

Table S6. The related EIS fitting parameters of NiO sample for OER.

Potential (V)	Rs	Rct	CPE1-T	CPE1-P	W1-R	W1-T	W1-P
1.1	1.896	0.30581	0.0027893	0.81778	0.9494	0.12407	0.3207
1.15	1.906	0.30591	0.0044723	0.76202	0.88019	0.12616	0.32667
1.2	1.899	0.26794	0.0039383	0.79303	1.014	0.21897	0.32705
1.25	1.891	0.28902	0.004907	0.7742	0.98815	0.23111	0.34351
1.3	1.886	0.31365	0.0048691	0.76803	1.054	0.26911	0.36736
1.35	1.877	0.35529	0.0065415	0.72746	0.91753	0.27906	0.38051
1.4	1.861	0.36784	0.0085388	0.7029	0.92846	0.47129	0.39794
1.45	1.847	0.37568	0.013076	0.66273	0.96201	0.66201	0.41399
1.5	1.839	0.37794	0.016692	0.63844	0.96061	0.75809	0.41469
1.55	1.835	0.36499	0.018738	0.63319	0.95219	0.8105	0.40016
1.6	1.832	0.34104	0.023074	0.62028	0.89745	0.81117	0.35139

Table S7. The related EIS fitting parameters of NiO sample for OER.

Potential (V)	Rs	Rct	CPE1-T	CPE1-P	W1-R	W1-T	W1-P
1.1	3.02	0.32502	0.0031751	0.76401	0.6334	0.041468	0.29142
1.15	2.89	0.30839	0.0023675	0.77733	0.84228	0.080437	0.30108
1.2	2.96	0.27224	0.0031099	0.76484	0.67435	0.069012	0.29331
1.25	2.911	0.44971	0.010823	0.6123	4.475	2.218	0.55328
1.3	2.883	0.46459	0.016028	0.57735	4.742	2.573	0.56693
1.35	2.724	0.28064	0.0066282	0.73761	0.69947	0.12551	0.30027
1.4	2.747	0.28563	0.0068586	0.73174	0.94263	0.27482	0.3281
1.45	2.741	0.35478	0.015005	0.64029	1.027	0.52338	0.40609
1.5	2.72	0.33039	0.013152	0.66506	1.2	0.79968	0.4272
1.55	2.715	0.3112	0.014689	0.66227	1.014	0.662	0.39143
1.6	2.696	0.3345	0.023885	0.61199	0.8089	0.52294	0.35555

Table S8. The calculated DFT energy, ZPE and TS of HMF and OH on Co_3O_4 (111) and $NiCo_2O_4$ (111) surfaces.

		E(total)	ZPE	TS	G
HMF	Co_3O_4 Co site	-612.35471833	2.962466	0.453499	-609.84575133
	$NiCo_2O_4$ Co site	-592.07955534	2.956818	0.548353	-589.67109034
	$NiCo_2O_4$ Ni site	-591.47586093	2.980203	0.458931	-588.95458893
OH	Co_3O_4 Co site	-526.73128963	0.314396	0.091998	-526.50889163
	$NiCo_2O_4$ Co site	-506.04384326	0.324152	0.109335	-505.82902626
	$NiCo_2O_4$ Ni site	-505.58735423	0.311344	0.111436	-505.38744623

Table S9. The calculated adsorption energy of HMF and OH on Co_3O_4 (111) and $NiCo_2O_4$ (111) surfaces.

		E(total)	E(surface)	E(molecule)	ΔE(ads)
HMF	Co_3O_4 Co site	-609.84575133	-515.26635498	-92.62330428	-1.95609207
	$NiCo_2O_4$ Co site	-589.67109034	-494.49289166	-92.62330428	-2.55489440
	$NiCo_2O_4$ Ni site	-588.95458893	-494.49289166	-92.62330428	-1.83839299
OH	Co_3O_4 Co site	-526.50889163	-515.26635498	-10.19637991	-1.04615674
	$NiCo_2O_4$ Co site	-505.82902626	-494.49289166	-10.19637991	-1.13975469
	$NiCo_2O_4$ Ni site	-505.38744623	-494.49289166	-10.19637991	-0.69817466

Table S10. The calculated intermediates energies on $NiCo_2O_4$ (111) surface at Co site, unit: eV.

	Energy	ZPE	TS	G	ΔG	Plot G
Surface	-494.492892	/	/	-494.492892	0.000000	0.000000
$C_6H_6O_3$*(HMF)	-592.079555	2.956818	0.548353	-589.671090	-2.554894	-2.554894
$C_6H_6O_4$*(HMFCA)	-598.994266	3.09813	0.579052	-596.475188	-0.653723	-3.208617
$C_6H_4O_4$*(FFCA)	-592.240267	2.468447	0.510337	-590.282157	-1.898978	-5.107596
$C_6H_4O_5$*(FDCA)	-599.376771	2.596473	0.52379	-597.304088	-0.871556	-5.979152
H_2O	-14.224359	0.567711	0.585737	-14.242385	2.554706	-3.424446
OH^-	-10.196380	/	/	-10.196380		
$C_6H_6O_3$ (g)	-95.220568	2.990311	0.393047	-92.623304		
$C_6H_4O_5$ (g)	-102.447856	2.66063	0.469264	-100.256490		

Table S11. The calculated intermediates energies on $NiCo_2O_4$ (111) surface at Ni site, unit: eV.

	Energy	ZPE	TS	G	ΔG	Plot G
Surface	-494.4928917	/	/	-494.4928917	0.0000000	0.0000000
$C_6H_6O_3$*(HMF)	-591.4758609	2.98020	0.45893	-588.9545889	-1.8383930	-1.8383930
$C_6H_6O_4$*(HMFCA)	-599.1229675	3.12279	0.56411	-596.5642915	-1.4593275	-3.2977205
$C_6H_4O_4$*(FFCA)	-592.1448480	2.47198	0.49318	-590.1660470	-1.6937653	-4.9914858
$C_6H_4O_5$*(FDCA)	-599.3767712	2.59647	0.52379	-597.3040882	-0.9876662	-5.9791520
H_2O	-14.2243588	0.56771	0.58574	-14.2423848	2.5547064	-3.4244456
OH^-	-10.1963799	/	/	-10.1963799		
$C_6H_6O_3$ (g)	-95.2205683	2.99031	0.39305	-92.6233043		
$C_6H_4O_5$ (g)	-102.4478562	2.66063	0.46926	-100.2564902		

Table S12. The calculated intermediates energies on Co_3O_4 (111) surface at Co site, unit: eV.

	Energy	ZPE	TS	G	ΔG	Plot G
Surface	-515.26635498	/	/	-515.2663550	0.0000000	0.0000000
$C_6H_6O_3$*(HMF)	-612.35471833	2.96247	0.45350	-609.8457483	-1.9560891	-1.9560891
$C_6H_6O_4$*(HMFCA)	-619.35320895	3.10203	0.53358	-616.7847590	-0.7886356	-2.7447247
$C_6H_4O_4$*(FFCA)	-612.89988356	2.47630	0.44996	-610.8735436	-2.1807944	-4.9255190
$C_6H_4O_5$*(FDCA)	-619.94837956	2.60078	0.51889	-617.8664896	-0.8425710	-5.7680900
H_2O	-14.2243588	0.56771	0.58574	-14.2423848	2.3436444	-3.4244456
OH^-	-10.1963799	/	/	-10.1963799		
$C_6H_6O_3$ (g)	-95.2205683	2.99031	0.39305	-92.6233043		
$C_6H_4O_5$ (g)	-102.4478562	2.66063	0.46926	-100.2564902		

Table S13. The calculated intermediates energies on $NiCo_2O_4$ (111) surface at Co site, unit: eV.

	Energy	ZPE	TS	G	ΔG	Plot G
Surface	-494.492892	/	/	-494.4928917	0.0000000	0.0000000
$C_6H_6O_3$*(HMF)	-592.079555	2.956818	0.548353	-589.6710903	-2.5548944	-2.5548944
$C_6H_4O_3$*(DFF)	-584.166818	2.481337	0.405167	-582.0906484	-0.5115679	-3.0664623
$C_6H_4O_4$*(FFCA)	-592.240267	2.468447	0.510337	-590.2821571	-2.0411336	-5.1075958
$C_6H_4O_5$*(FDCA)	-599.376771	2.596473	0.52379	-597.3040882	-0.8715561	-5.9791520
H_2O	-14.224359	0.567711	0.585737	-14.2423848	2.5547064	-3.4244456
OH^-	-10.196380	/	/	-10.1963799		
$C_6H_6O_3$ (g)	-95.220568	2.990311	0.393047	-92.6233043		
$C_6H_4O_5$ (g)	-102.447856	2.66063	0.469264	-100.2564902		

Table S14. The calculated intermediates energies on $NiCo_2O_4$ (111) surface at Ni site, unit: eV.

	Energy	ZPE	TS	G	ΔG	Plot G
Surface	-494.4928917	/	/	-494.4928917	0.0000000	0.0000000
$C_6H_6O_3$*(HMF)	-591.4758609	2.98020	0.45893	-588.9545889	-1.8383930	-1.8383930
$C_6H_4O_3$*(DFF)	-583.9633017	2.35228	0.46383	-582.0748567	-1.2122775	-3.0506705
$C_6H_4O_4$*(FFCA)	-592.1448480	2.47198	0.49318	-590.1660470	-1.9408153	-4.9914858
$C_6H_4O_5$*(FDCA)	-599.3767712	2.59647	0.52379	-597.3040882	-0.9876662	-5.9791520
H_2O	-14.2243588	0.56771	0.58574	-14.2423848	2.5547064	-3.4244456
OH^-	-10.1963799	/	/	-10.1963799		
$C_6H_6O_3$ (g)	-95.2205683	2.99031	0.39305	-92.6233043		
$C_6H_4O_5$ (g)	-102.4478562	2.66063	0.46926	-100.2564902		

Table S15. The activity comparison of CO_2RR-HMFOR device.

Electrocathode-CO_2RR		Electroanode-HMFOR		CO_2RR-HMFOR device activity		
cathode catalyst	reduced product	anode catalyst	oxidation product	E_{cell}	j (mA cm^{-2})	Ref.
Au	**H_2 (28.5%) and CO (66.1%) FE = 94.7%**	**$NiCo_2O_4$**	**FDCA (FE=91.9%)**	**1.70**	**4.5**	**This work**
PdO_x/ZIF-8	CO FE = 97%	PdO_x/ZIF-8	maleic acid (20.0%) and formic acid (64.3%) FE = 84.3%	2.70	160	[1]
Cu_1Bi	HCOOH FE = 90%	NiCoLDHs	FDCA FE = 85%	2.35	150	[2]
Bi-In/C	HCOOH FE = 85.1%	$Ni(OH)_2$/Ni foam	FDCA FE = 88.2%	2.05 (a solar cell)	11.58	[3]
Cu_2O/Cu-NF@Cu	C_2H_4 FE = 74.5%	CuO-NF@Cu	FDCA FE = 96.6%	2.75	188.8	[4]
InOOH-O_V	HCOOH FE =87.5%	InOOH-O_V	FDCA FE = 91.6%	2.27	10	[5]
Bi@C-700-4	HCOOH FE = 94.8%	Bi@C-700-4	FDCA FE = 81.2%	2.06 (a solar cell)	10.64	[6]
CuO/TiB2-GDL	C_2H_4 FE = 49.2%	$Ni(OH)_2$@NF	FDCA FE = 85.4%	1.40	400	[7]

Table S16. Comparison of full-cell energy efficiency of various catalysts during CO_2 electroreduction.

cathode catalyst	E_{cell}	j(mA cm^{-2})	reduced product	EE (%)	Ref
Au	**1.70**	**4.5**	**H_2 (28.5%) and CO (66.1%) FE = 94.7%**	**FDCA (22.2%), CO (15.9%) and H_2 (5.2%) EE_{total} = 43.3%**	**This work**
Er SAC-Flow cell	-	50	CO (≥90%)	42.2	[8]
Er SAC-MEA	-	50	CO (≥90%)	43.2	
NiNC-IMI-AEM	-3.0	-200	CO (100%)	~40	[9]
PT/Cu-GDE	-	-2000	C_{2+} (85%)	＞50	[10]
$Cu_{0.9}Zn_{0.1}$	3.7	-150	C_{2+} (91±2%)	28-32	[11]
$Cu_2(OH)_3F$	-	-700	C_{2+} (93%) Ethanol (50%)	Ethanol (30%)	[12]
CG-medium Cu	3.3	100	C_{2+} (80%)	28	[13]
PFSA modifed Cu	3.6	200	C_2 (75%)	25	[14]
EC-Cu	-	200	C_{2+} (75%) ethylene (60%)	C_{2+} (30%) ethylene (20%)	[15]

References:

(1) J. Bi, Q. Zhu, W. Guo, P. Li, S. Jia, J. Liu, J. Ma, J. Zhang, Z. Liu, B. Han, *ACS Sustainable Chem. Eng.,* 2022, **10**, 8043–8050.

(2) S.-Q. Liu, M.-R. Gao, S. Wu, R. Feng, Y. Wang, L. Cui, Y. Guo, X.-Z. Fu, J.-L. Luo, *Energy Environ. Sci.,* 2023, **16**, 5305–5314.

(3) X. Cao, B. Wulan, Y. Wang, J. Ma, S. Hou, J. Zhang, *Sci. Bull*., 2023, **68**, 1008–1016.

(4) Z. Zhang, S. Liu, Z. Wu, X. Chen, J. Wang, Y. Gao, S. Wang, F. Tao, G. Lv, *Green Chem.,* 2023, **25**, 5404–5415.

(5) F. Ye, S. Zhang, Q. Cheng, Y. Long, D. Liu, R. Paul, Y. Fang, Y. Su, L. Qu, L. Dai, C. Hu, *Nat. Commun.,* 2023, **14**, 2040.

(6) W. Guo, X. Cao, D. Tan, B. Wulan, J. Ma, J. Zhang, Angew. Chem. Int. Ed. 2024, **63**, e202401333.

(7) C. Lu, P. Shi, S. Huang, C. Yang, J. Zhu, J. Zhang, C. Ke, Y. Su, X. Zhuang, T. Wang, *Angew. Chem. Int., Ed*. 2025, **64**, e202423263.

(8) Q. Wang, T. Luo, X. Cao, Y. Gong, Y. Liu, Y. Xiao, H. Li, F. Gröbmeyer, Y.-R. Lu, T.-S. Chan, C. Ma, K. Liu, J. Fu, S. Zhang, C. Liu, Z. Lin, L. Chai, E. Cortes, M. Liu, *Nat. Commun.,* 2025, **16**, 2985.

(9) S. Brückner, Q. Feng, W. Ju, D. Galliani, A. Testolin, M. Klingenhof, S. Ott, P. Strasser, *Nat. Chem. Eng.,* 2024, **1**, 229–239.

(10) J. Chen, H. Qiu, Y. Zhao, H. Yang, L. Fan, Z. Liu, S. Xi, G. Zheng, J. Chen, L. Chen, Y. Liu, L. Guo, L. *Nat. Commun.,* 2024, **15**, 5893.

(11) J. Zhang, C. Guo, S. Fang, X. Zhao, L. Li, H. Jiang, Z. Liu, Z. Fan, W. Xu, J. Xiao, M. Zhong, *Nat. Commun.,* 2023, **14**, 1298.

(12) Y. Da, J. Chen, L. Fan, R. Jiang, Y. Xiao, M. Wang, G. Chen, Z. Tian, H. Zhang, H. Jin, X. Chen, C. Ji, S. Xi, Y. Lum, L. Wang, T. Zhu, J. Zhang, W. Chen, *Angew. Chem. Int. Ed*., 2025, e202506867.

(13) M. Fan, J. E. Huang, R. K. Miao, Y. Mao, P. Ou, F. Li, X.-Y. Li, Y. Cao, Z. Zhang, J. Zhang, Y. Yan, A. Ozden, W. Ni, Y. Wang, Y. Zhao, Z. Chen, B. Khatir, C. P. O'Brien, Y. Xu, Y. C. Xiao, G. I. N. Waterhouse, K. Golovin, Z. Wang, E. H. Sargent, D. Sinton, *Nat. Catal.*, 2023, **6**, 763–772.

(14) Y. Zhao, L. Hao, A. Ozden, S. Liu, R. K. Miao, P. Ou, T. Alkayyali, S. Zhang, J. Ning, Y. Liang, Y. Xu, M. Fan, Y. Chen, J. E. Huang, K. Xie, J. Zhang, C. P. O'Brien, F. Li, E. H. Sargent, D. Sinton, *Nat. Synth.,* 2023, **2**, 403–412.

(15) Y. Cao, Z. Chen, P. Li, A. Ozden, P. Ou, W. Ni, J. Abed, E. Shirzadi, J. Zhang, D. Sinton, J. Ge, E. H. Sargent, *Nat. Commun.,* 2023, **14**, 2387.